Molecular Therapy
Nucleic Acids
Original Article

Discovery of peptides for ligand-mediated delivery of mRNA lipid nanoparticles to cystic fibrosis lung epithelia

Melissa R. Soto,[1] Mae M. Lewis,[2] Jasmim Leal,[1] Yuting Pan,[1] Rashmi P. Mohanty,[1] Arian Veyssi,[2] Esther Y. Maier,[3] Brittany J. Heiser,[2] and Debadyuti Ghosh[1]

[1]Division of Molecular Pharmaceutics and Drug Delivery, College of Pharmacy, The University of Texas at Austin, 2409 University Avenue, Austin, TX 78712, USA; [2]Department of Biomedical Engineering, The University of Texas at Austin, 107 W. Dean Keeton St., Austin, TX 78712, USA; [3]College of Pharmacy, The University of Texas at Austin, 2409 University Avenue, Austin, TX 78712, USA

For cystic fibrosis patients, a lung-targeted gene therapy would significantly alleviate pulmonary complications associated with morbidity and mortality. However, mucus in the airways and cell entry pose huge delivery barriers for local gene therapy. Here, we used phage display technology to select for and identify mucus- and cell-penetrating peptides against primary human bronchial epithelial cells from cystic fibrosis patients cultured at the air-liquid interface. At the air-liquid interface, primary human bronchial epithelial cells produce mucus and reflect cystic fibrosis disease pathology, making it a clinically relevant model. Using this model, we discovered a lead candidate peptide and incorporated it into lipid nanoparticles to deliver mRNA to primary human bronchial epithelia *in vitro* and mouse lungs *in vivo*. Compared to lipid nanoparticles without our peptide, peptide-lipid nanoparticles demonstrated up to 7.8-fold and 3.4-fold higher reporter luciferase bioactivity *in vitro* and *in vivo*, respectively. Importantly, these peptides facilitated higher specific uptake of nanoparticles into lung epithelia relative to other cell types. Since gene delivery to primary human bronchial epithelia is a significant challenge, we are encouraged by these results and anticipate that our peptide could be used to successfully deliver cystic fibrosis gene therapies in future work.

INTRODUCTION

Cystic fibrosis (CF) is a genetic disease in which single mutations occur within the CF transmembrane conductance regulator (CFTR) gene, and as a result requires gene therapy to correct the mutation and restore CFTR function. While these mutations affect all organs, mucus buildup found in the lungs of CF patients results in the most severe lung morbidities, which are the leading cause of death for CF patients.[1,2] As a result, many efforts focus on developing gene-therapy formulations that can be locally delivered to the lungs.[3] However, the hostile environment found in CF patients' lungs, which includes hyperconcentrated mucus and immune cells such as macrophages, greatly hinders treatments from reaching intended target sites (i.e., cells harboring the CFTR mutation). Given that the thick mucus layer and cell membrane are two of the biggest barriers to successful gene delivery, it is necessary to develop gene-therapy carriers that can overcome these obstacles.

Traditionally, clinics have used virus vectors for CF gene therapy due to their intrinsic ability to enter mammalian cells. However, their use can be limited due to their innate immunogenicity, broad tropism, and limited size capacity for packaging nucleic acids.[3–5] Due to these challenges, non-viral delivery systems are alternative carriers but are often blocked by the various extracellular and intracellular barriers of uptake (i.e., mucosal and cell membrane). To overcome the mucus barrier, researchers have enhanced non-viral delivery systems by formulating with higher amounts of mucus-penetrating polymers, such as polyethylene glycol (PEG). However, PEGylation can hinder cellular uptake, and PEG alone does not have inherent cell-targeting capabilities.[6] Peptides are attractive alternative delivery systems, since they can shuttle therapeutics to their intended target site, potentially enhance cell internalization, and be easily incorporated into non-viral delivery systems where larger payloads can be used.[7]

To achieve targeted delivery, researchers have used directed evolution to select virus variants with redirected tropism or discover cell-targeting peptides through technologies such as phage display. For example, groups have evolved adeno-associated viruses and lentiviruses to target human CF epithelia and improve the transduction of mammalian viral delivery systems.[8–10] For phage display, on the other hand, M13 or T7 bacterial viruses, i.e., phage, are traditionally used as screening tools to discover peptides with desired properties. Here, phage are genetically engineered to display recombinant random peptides or proteins on their viral coat proteins (i.e., capsid proteins). For instance, T7 phage can be genetically modified to display up to 415

Received 27 March 2024; accepted 25 October 2024;
https://doi.org/10.1016/j.omtn.2024.102375.

Correspondence: Debadyuti Ghosh, Division of Molecular Pharmaceutics and Drug Delivery, College of Pharmacy, The University of Texas at Austin, 2409 University Avenue, Austin, TX 78712, USA.
E-mail: dghosh@austin.utexas.edu

A

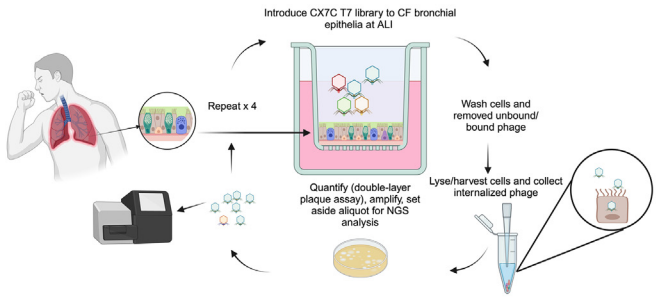

B

Round	Incubation	Wash Steps	MOI (vg/cell)
1	16 h	Elution Buffer (EB) x 20 min → 7 DPBS Wash steps	1000
2	4 h	EB x 20 min → DPBS x 20 min → 6 additional DPBS washes	1000
3	1 h	EB x 20 min → DPBS x 20 min → 6 additional DPBS washes	1000
4	1 h	EB x 20 min → DPBS x 20 min → 6 additional DPBS washes	1000
5	1 h	EB x 20 min → DPBS x 20 min → 6 additional DPBS washes	1000

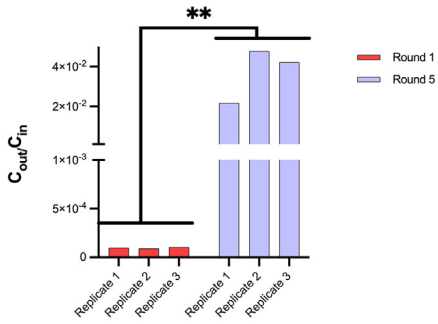

Figure 1. Panning strategy and T7 phage display library enrichment

(A) Selection strategy using a cysteine constrained random 7-amino-acid peptide T7 phage display library (CX_7C) against differentiated primary human bronchial epithelial cells (pHBECs) through iterative, high-throughput selection for a total of five rounds. Image made with BioRender. (B) Selection conditions (left) and enrichment (right) of CX_7C phage library for enhanced CF pHBEC uptake. C_{out} represents the concentration of phage collected after each round, and C_{in} is the initial input phage concentration. Phage were added at 1,000 viral genomes/cell (vg/cell) and incubated for 16 h at 37°C for round 1 and 1 h at 37°C for round 5 (see also Figure S1). Data represent change in C_{out}/C_{in} for three separate replicates from the first to last round of selection. Unpaired t test, $^{**}p = 0.0094$.

copies of a single peptide on the surface of their capsids, and phage libraries can be created that consist of up to 10^9–10^{10} unique peptide-presenting phage or "clones." Pooled together, these random peptide-presenting phage libraries can be incubated or "panned" against a target of interest.[11] Through iterative rounds of panning against the target, there is a selection pressure applied such that peptide(s) with the desired properties are identified. After identification, peptides are typically removed from the structural context of the phage and incorporated into delivery systems (e.g., antibodies, lipid nanoparticles [LNPs], viruses) to redirect targeting.[12–16] In the context of respiratory targeting, multiple groups have demonstrated the utility of phage display for discovering peptides that can target the lungs, both systemically and locally.[14,16–18] For CF therapy specifically, Romanczuk et al. panned phage display libraries against primary human bronchial epithelial cells (pHBECs); however, panning was done with pHBECs from non-CF donors in solution, meaning these cells were not fully demonstrative of CF airway conditions *in vivo*.[14]

For CF gene therapy, it is necessary to identify ligands that overcome mucus and cellular barriers to facilitate targeted delivery to affected CF airway epithelia. While in earlier work we identified mucus-penetrating peptides by panning our custom T7 phage display library against an *in vitro* CF-like mucus model,[19] this strategy focused on mucus penetration in a synthetic disease model and did not fully address the challenges of targeting and entering the airway epithelia in clinically relevant models. To address these critical issues, we leveraged directed evolution with phage display to discover and select for peptides with the desired physicochemical properties to achieve both mucus and cell penetration. Here, we used T7 phage display to pan against fully differentiated pHBECs isolated from CF patients, which produce mucus, have ciliated cells, and phenotypically and physiologically represent a more disease-relevant model to mimic conditions found in the lungs of CF patients.[20] With this strategy, our goals were to identify peptides and their physicochemical properties and confirm that they improve phage uptake into mucus-producing pHBECs. Additionally, we aimed to demonstrate that select peptide candidates could be incorporated into clinically relevant LNPs to improve mRNA LNP transfection *in vitro* in fully differentiated CF patient cells and *in vivo* in lungs via pulmonary delivery.

RESULTS

Selection of enriched mucus- and cell-penetrating T7 phage clones

For our selection strategy, we iteratively panned a cysteine-constrained cyclic T7 7-mer (CX_7C) peptide-presenting phage library against mucus-producing pHBECs. Specifically, we used pHBECs cultured at physiologically relevant air-liquid interface (ALI) to identify phage that can overcome two main delivery barriers in the airway space for CF therapy: (1) mucosal barrier and (2) cellular barrier. We chose pHBECs isolated from seven CF patients (Table S1) that were pooled and cultured at ALI as our selection model, since it more accurately reflects the CF microenvironment upon differentiation (i.e., mucus production and subsequent ciliary movement). An overview of our selection strategy is depicted in Figure 1A. To increase selection pressure throughout our rounds of panning, we sequentially shortened incubation times from round 1 to round 3 and increased the time cells were incubated in wash buffer from round 1 to round 2 (selection details from each round are shown in Figure 1B). Additionally, cells were not washed after round 1 to allow for mucus buildup in subsequent rounds and to increase selection pressure. Alcian blue staining of pHBECs confirmed that the volume administered and incubation period during the last round of selection did not remove the

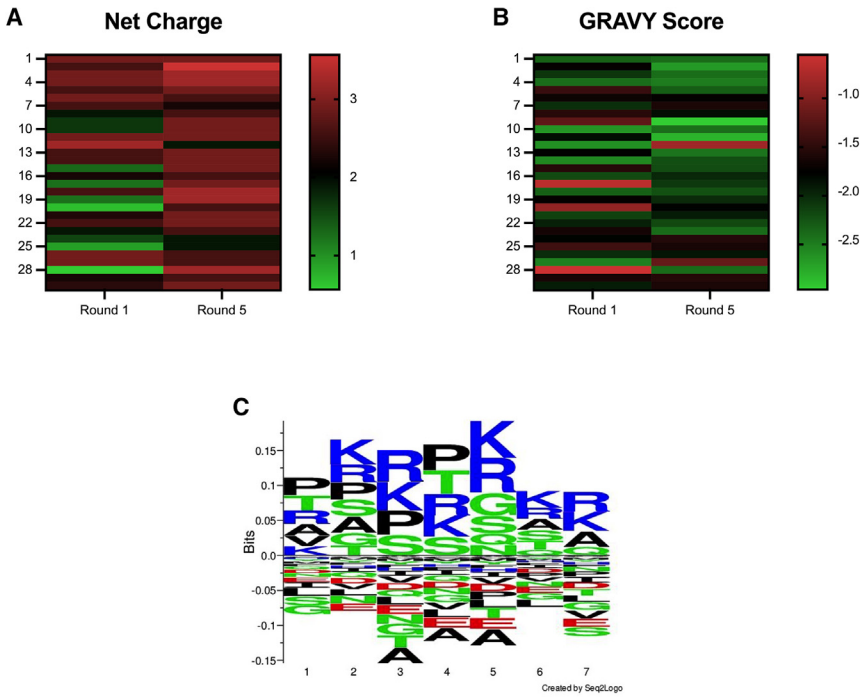

Figure 2. Physicochemical properties of peptides displayed on enriched phage

(A) Net charge and (B) GRAVY score values were calculated for the top 30 most frequent peptide sequences from each replicate (n = 3); total of 90 sequences analyzed per round. Peptides were ranked 1–30 based on frequency. Graphed are the mean values for each ranked peptide sequence (n = 3). (C) Multiple sequence alignment visual representation using Seq2Logo for the top 30 sequences of each replicate after five rounds of selection.[22]

mucus layer (Figure S1). We next quantified internalized phage after each round of selection by standard double-layer plaque assay to determine enrichment following each round of selection. To ensure that we quantified primarily internalized phage, we washed cells extensively, lysed cells to collect the internalized phage, and separated cell lysate from cell debris by centrifugation. After five rounds of selection, we saw an average 380-fold increase in C_{out}/C_{in} (ratio of concentration of phage internalized or "output" to concentration of input phage), demonstrating that our CX_7C T7 library was enriched (Figure 1B).

Enriched clones display peptides that are positively charged and hydrophilic

Using next-generation sequencing (NGS) and a custom python script for data analysis,[19,21] we identified "hits," or the top 30 most abundant peptide sequences from each round of selection, and ranked these peptides from 1 to 30 (n = 3). For each ranked peptide (n = 3), we calculated and compared its net charge, i.e., for each peptide, the sum of charges for each ionizable group (from rounds 1 and 5), to determine whether there was a shift in net charge after all rounds of selection. A heatmap depicting these values indicates that the average net charge of peptides shifted to a slightly more positive value from round 1 to round 5 (Figure 2A).

Similarly, we calculated and compared the grand average of hydropathicity, or GRAVY score,[23] from the top 30 most frequently occurring peptide sequences from rounds 1 and 5 (Figure 2B). The more positive the GRAVY score, the more hydrophobic the peptide sequence, and vice versa. Here, we also observed a shift from the first to last round of selection to a slightly more negative GRAVY score, indicating that there were more hydrophilic sequences present after five rounds of selection (Figure 2B).

Additionally, we implemented the Seq2Logo tool to visualize a multiple sequence alignment for the top 30 sequences of all replicates (n = 3) after the fifth round of selection and identify the amino acid frequency at each position of the 7-mer peptide.[22] We observed that this consensus sequence was rich in the basic and hydrophilic amino acids arginine and lysine, which further supported trends we saw for net charge and GRAVY scores (Figure 2C).

Lastly, we further analyzed these sequences to select individual clones for further validation. From each replicate, we selected clones that were within the top ten most abundant sequences in the fifth round of selection and found in all three replicates (Table 1). We observed that each clone showed an increase in their abundance, i.e., percentage of total sequences identified from NGS analysis after each subsequent round (Figure 3A). The enrichment of relative frequency of individual clones ranged from ∼7.7 (clone B) to 13.7 (clones C and E) from the first to fifth round. Except for clone F, net charges were 2.9 and GRAVY scores were less than −2.0. Clone F had a net charge and GRAVY score of 0.9 and −0.26, respectively. Additionally, we used the SAROTUP (scanner and reporter of target-unrelated peptides) suite to confirm that these selected peptides are unique compared to previously identified peptides from biopanning and are not target-unrelated peptides.[24–26] Furthermore, we used the Immune Epitope Database (https://www.iedb.org/home_v3.php) as a tool to ensure that the peptides used for validation did not match any known epitopes studied in humans.

Enriched clones demonstrate improved uptake through mucus-producing cystic fibrosis primary human bronchial epithelial cells

Like our panning procedure, we differentiated our pooled pHBECs (see materials and methods) and incubated them with the individual peptide-presenting phage clones that we identified during the selection process (Table 1) to confirm that these clones achieve both

Table 1. T7 phage clones selected for validation and the physicochemical properties of their displayed peptides

Clone identifier	Sequence	R1 to R5 enrichment	Net charge	GRAVY score
A	CTPKRSRAC	8.082	2.9	−2.03
B	CTRPTRSKC	7.657	2.9	−2.39
C	CTSTRKKQC	13.713	2.9	−2.57
D	CPAPRGKRC	8.836	2.9	−2.10
E	CAPSKRNRC	13.745	2.9	−2.43
F	CLSPTGKAC	12.630	0.9	−0.26
CPS	CPSSSREKC	–	1	−1.21
Wild type (WT)	–	–	–	–
Naive library (NL)	CXXXXXXXC	–	–	–

mucus penetration and cell uptake (Figure 3B). From our validation study, we found that of the six clones validated, clones B–E demonstrated a significant difference in uptake compared to an unselected naive library control ($p < 0.05$). Additionally, clones B, C, and E had significantly improved uptake compared to a peptide insertless wild-type (WT) control and an internal control sequence (denoted as CPS) (Table 1). Clone CPS was previously discovered in our lab from phage display screening for improved diffusion through CF-like mucus.[19] Our best performing clone, clone C, demonstrated ∼454-fold ($p < 0.0005$), 56-fold ($p < 0.005$), and 50-fold ($p < 0.005$) improvement in uptake compared to naive library, WT, and clone CPS, respectively.

Peptides can be successfully incorporated into lipid nanoparticles

We confirmed that peptides could improve transport and intracellular uptake in CF pHBECs while in the context of a phage particle. Next, we sought to determine whether these peptides could be effectively incorporated into an LNP formulation. We encapsulated nanoluciferase (NLuc) reporter mRNA into LNPs (NLuc LNPs) via microfluidic mixing using the four lipids in Moderna's Food and Drug Administration (FDA)-approved Spikevax formulation as our base composition (Table 2). Based on its abundance and validation in phage uptake, we selected Peptide C from clone C to introduce into LNPs for subsequent studies. We used either Peptide C or a control mucus-penetrating peptide, CPS, conjugated to a myristic acid fatty acid as peptide-lipids to incorporate into LNPs as a fifth component lipid. Peptide-lipids or additional PEG-lipid (to serve as an additional mucus-penetrating control) were added to Moderna's Spikevax base composition at an optimized percentage (Table 2). In brief, all lipid components (including peptide-lipid conjugates) were dissolved in an organic phase and microfluidically mixed with mRNA in aqueous phase using a Y-shaped staggered herringbone mixer.[27] After formulating LNPs, dynamic light scattering (DLS) data showed that all formulations had diameter sizes below 80 nm (Figure 4A). The polydispersity index (PDI), which approximates the monodispersity of the formulations, was highest for our PEG formulation, while all other formulations had PDIs of <0.2 (Figure 4A). Next, we characterized their encapsulation efficiencies (EEs); all but the PEG-LNP formulation resulted in EEs >90% (Figure 4A). Next, we determined the zeta potential values of our four LNP formulations (Figure 4A). We observed that incorporation of our Peptide C-lipid shifted the zeta potential to a more positive value compared to all three other formulations. Lastly, we imaged Peptide C-LNPs using transmission electron microscopy (TEM) and observed no noticeable differences in LNP morphology after incorporating the Peptide C-lipid component (Figure S2).

Selected peptide functionalized lipid nanoparticles enhance luciferase bioactivity

After confirming that peptides could be incorporated into LNPs, we determined how each formulation affected mRNA LNP transfection. We delivered NLuc-LNPs to differentiated pHBECs pooled from seven different donors (i.e., cultured at ALI) and incubated for 48 h before measuring bioluminescence. Here, we saw significantly enhanced NLuc bioactivity between Peptide C-LNPs and all other formulations (Figure 4B). Specifically, we observed a 10.5-fold and 4.5-fold increased luminescence from mRNA delivered

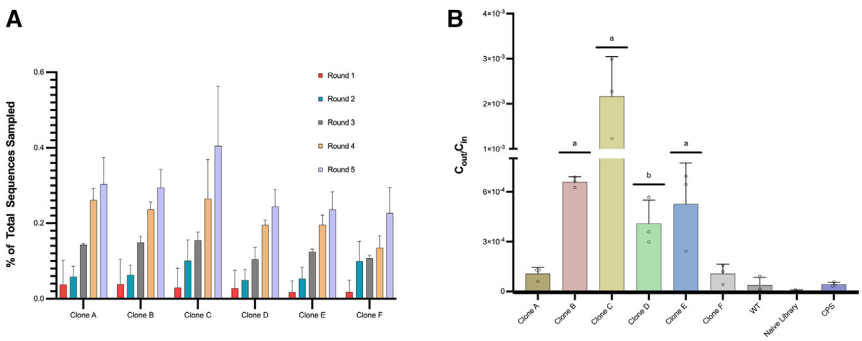

Figure 3. Enrichment and validation of individual clones identified using high-throughput sequencing data obtained from NGS

(A) We identified peptide-displaying clones that were present in the top ten most abundant sequences across all three replicates. For each round of panning, the percentage of total sequences sampled represents the (average peptide frequency count/total number of sequences obtained from NGS data) × 100 ($n = 3$; mean [SD]). (B) We validated clones using a standard double-layer plaque assay. C_{out} represents the output concentration of phage collected from pHBECs cultured at ALI after 1 h, and C_{in} is the initial input phage concentration. Controls include wild-type (WT) phage which lacks peptides on its capsid surface, naive library which is a mixture of 7-mer peptide presenting phage clones, and a mucus-penetrating clone displaying the peptide sequence CPSSSREKC (denoted as CPS; net charge 1 and GRAVY score of −1.2) ($n = 3$, mean [SD; one-way ANOVA (Kruskal-Wallis test; uncorrected Dunn's)); a: significant difference from all control groups; b: significant difference from naive library control group only ($p < 0.05$).

Table 2. LNP formulation details

Formulation	N/P	CIL	Helper lipid	PEG lipid	Peptide-lipid (PL)	CIL (%)	Helper (%)	Cholesterol (%)	PL (%)	PEG (%)	Molar % sum
Spikevax	6	SM-102	DSPC	DMG-PEG	–	50.00	10.00	38.50	0.00	1.50	100.00
Peptide C	6	SM-102	DSPC	DMG-PEG	Myr-C	46.88	9.38	36.09	6.25	1.41	100.00
PEG	6	SM-102	DSPC	DMG-PEG	–	46.88	9.38	36.09	0.00	7.66	100.00
CPS	6	SM-102	DSPC	DMG-PEG	Myr-CPS	46.88	9.38	36.09	6.25	1.41	100.00

N/P, nitrogen-to-phosphate ratio; CIL, cationic ionizable lipid; PEG, polyethylene glycol; DMG-PEG, 1,2-dimyristoyl-rac-glycero-3-methoxypolyethylene glycol-2000; DSPC, distearoylphosphatidylcholine; Myr, myristoyl group.

by Peptide C-LNPs compared to LNPs containing additional PEG-lipid or a CPS-conjugated lipid, respectively. Additionally, cells transfected with Peptide C-LNPs demonstrated 7.8-fold higher bioluminescence than Moderna's Spikevax-LNP. Lastly, we compared Peptide C-LNP to Spikevax across individual CF donors used in our selection process to assess whether we observed a similar trend in enhanced NLuc bioactivity while also acknowledging the variability between patients (Figure S3). Here, we saw that the average bioluminescence trended higher than Spikevax for all donors tested (Figure S3).

To determine whether our Peptide C-LNPs demonstrated preferential transfection in primary HBECs, we measured LNP transfection in an alternative cell model, a THP-1-derived human macrophage cell line. Using an incubation time (i.e., 48 h) similar to that in our validation study on pHBECs, we observed significantly lower NLuc bioluminescence (1.7-fold) from Peptide C-LNP groups compared to Spikevax-LNP treatment groups. Bioluminescence from cells transfected with Peptide C-LNPs was slightly lower than from our CPS-LNP group and slightly higher (but not statistically different) than from the PEG-LNP-treated group (Figure 4C).

Selected peptide functionalized lipid nanoparticles enhance luciferase bioactivity *in vivo*

Next, we sought to determine how our Peptide C could enhance delivery and NLuc bioactivity *in vivo* in BALB/c mice. We delivered LNP formulations intratracheally (IT) and harvested lungs after 24 h. We observed a trend similar to that in our *in vitro* ALI transfection study—cells transfected with our Peptide C formulation group showed the highest bioluminescence, followed by CPS-LNP, Spikevax-LNP, PEG-LNP, and lastly the PBS group (Figures 5A and 5B). Compared to Spikevax, Peptide C-LNPs demonstrated 3.4-fold higher bioluminescence. Notably, we also observed bioluminescence signals distributed throughout all lobes for our Peptide C-LNP group (Figure 5A). For our PEG-LNPs, we saw a ∼34.9-fold overall decrease in bioactivity compared to Peptide C *in vivo* (Figure 5B).

Lastly, given that we selected for a peptide that can cross both mucus and cell barriers, we wanted to ensure that NLuc mRNA bioactivity remained in the lungs following IT administration and avoided systemic expression in other organs. To this end, we administered either Peptide C-LNPs or PBS and compared the tissue biodistribution of NLuc mRNA bioactivity. For Peptide C-LNP-treated mice, we found

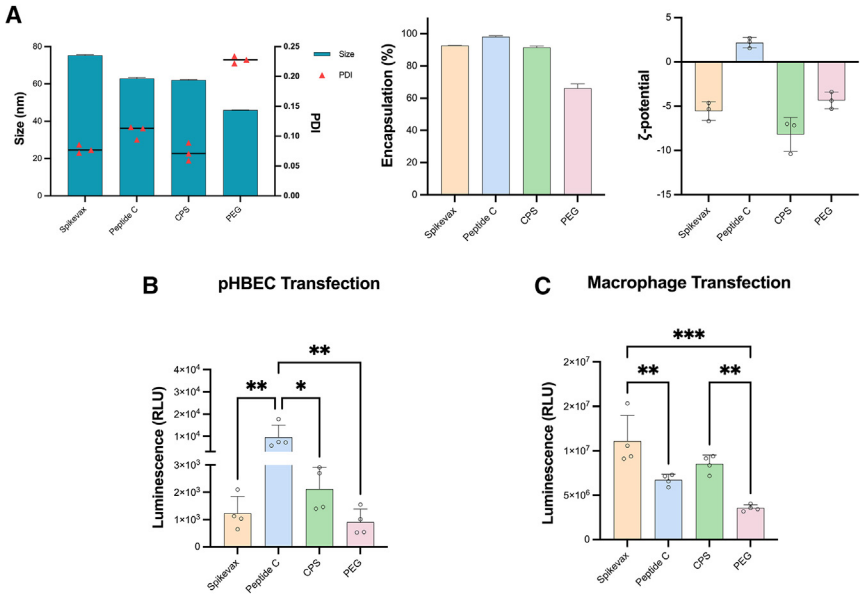

Figure 4. Characterization of LNPs and NLuc bioactivity in primary HBECs following LNP treatment

(A) We determined size in nanometers (nm), polydispersity index (PDI) by dynamic light scattering (DLS) (n = 3; mean [SD]), encapsulation efficiencies by modified Ribogreen assay (n = 2; mean [SD]), and zeta potential (n = 3; mean [SD]) (see also Figure S2). (B and C) We added LNPs (450 ng of mRNA) to the apical side of differentiated primary HBECs (n = 4; mean [SD]); one-way ANOVA (Tukey's multiple comparisons test), $^{*}p < 0.05$, $^{**}p < 0.01$ (see also Figure S3) (B) or THP-1 derived macrophages (n = 4; mean [SD]); one-way ANOVA (Tukey's multiple comparisons test), $^{**}p < 0.01$, $^{***}p < 0.001$ (C) and incubated them at 37°C for 48 h. Following incubation, we measured bioluminescence by plate reader.

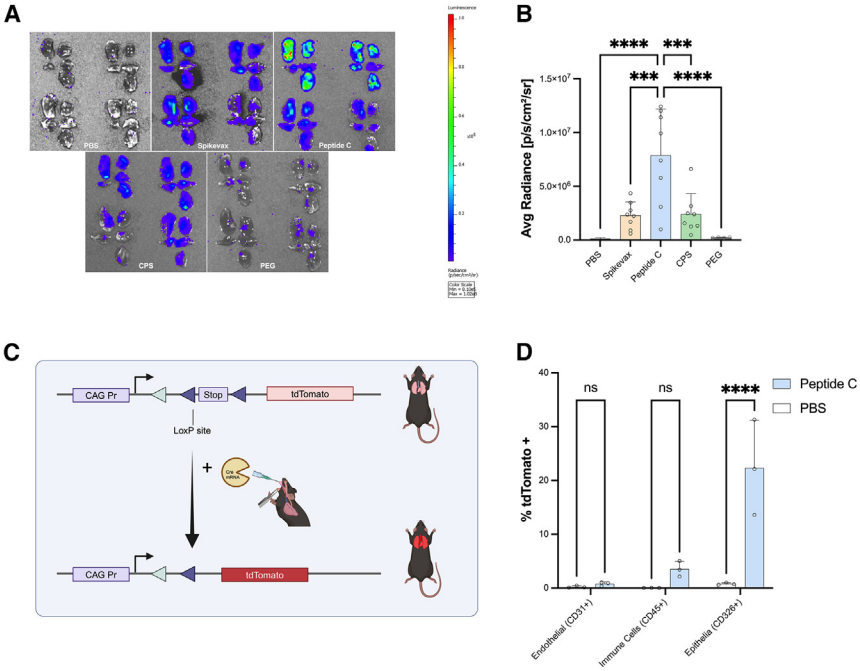

Figure 5. NLuc and Cre mRNA delivery following intratracheal administration of LNPs *in vivo*

(A) To BALB/c mice, we delivered 40 μL of either PBS or LNPs formulated at 20 ng/μL, harvested lungs at 24 h post administration, and immediately measured bioluminescence via IVIS imaging. Shown are representative images for each treatment group (n = 4–8; 6–8 weeks old). (B) Average radiance (p/s/cm^2/sr) was calculated for each lung. Data were pooled from two independent experiments (n = 4–8; mean [SD]); one-way ANOVA (Tukey's multiple comparisons test), ***$p < 0.0005$, ****$p < 0.0001$. (C) Schematic of Cre mRNA delivery to Ai9 mice. Image made with BioRender. (D) Flow-cytometry analysis of tdTomato-positive cells in various cell types in the lungs following intratracheal delivery of Cre mRNA to Ai9 mice (n = 3; mean [SD]); multiple unpaired t tests (Holm-Šídák multiple comparisons test), ****$p < 0.0001$. See also Figures S4 and S5.

robust and significantly higher mRNA bioactivity in only the lungs versus all other organs (brain, heart, kidneys, liver, spleen, and gastrointestinal [GI] tract) (Figure S4).

Peptide functionalized lipid nanoparticles can facilitate genome editing of desired cells *in vivo*

Next, we sought to determine whether we can apply peptide-LNPs to gene editing *in vivo*. For this study, we used B6.Cg-Gt(ROSA)26Sortm9(CAG-tdTomato)Hze/J (Ai9) mice, which contain a *LoxP* flanked STOP cassette that prevents robust expression of a tdTomato reporter gene downstream.[28] When Cre recombinase is introduced, it excises the STOP cassette and tdTomato is overexpressed. This conditional expression is seen as a proxy for gene editing, since cells that are effectively edited will express tdTomato and fluoresce (Figure 5C). Here, we intratracheally delivered Cre recombinase mRNA (Cre mRNA) using our Peptide C-LNP formulation to Ai9 mice and harvested lungs for flow-cytometry analysis 72 h after administration. For Peptide C-LNP-treated mice, we observed significantly higher tdTomato expression in epithelia compared to PBS-treated mice and observed 6.3-fold and 29.1-fold higher expression in epithelia compared to immune cells and endothelia, respectively (Figure 5D). Compared to PBS-treated mice, we also did not observe significantly higher tdTomato-positive cells for non-targeted cell types (i.e., endothelia and immune cells). Lastly, we observed no significant differences in cytotoxicity between the two treatment groups (Figure S5).

DISCUSSION

For diseases affecting the lungs, such as CF, local delivery of therapeutics is promising because it requires a lower dose compared to systemic delivery resulting in fewer side effects, and therapeutics can be administered in multiple ways that are amenable to outpatient use (e.g., nebulizer, dry powder, metered-dose inhaler).[29–33] For example, when comparing inhalation versus oral delivery of the same drug substance, lung/plasma drug concentration ratios can reach over 100 (compared to 1.6 for oral administration), making local delivery advantageous for targeting lung tissues.[33] For CF, this pharmacokinetic profile is attractive for the delivery of gene therapies such as CFTR gene addition or correcting specific CFTR mutations. However, both mucus and cell barriers hinder transport and delivery of therapeutics into the cell.[34–38] Common non-viral approaches for overcoming these barriers include the use of polymers (i.e., PEG, poly(β-amino ester)s [PBAEs]),[39–44] cationic lipids,[45,46] and novel ionizable lipids[47–50] that can be incorporated into nanoparticle systems (e.g., liposomes, LNPs, nanocomplexes). On their own, these components can confer significant advantages in mucus penetration (i.e., PEG) and enhanced cellular uptake (i.e., PBAEs, ionizable lipids), but often lack a combination of mucus, cell penetration, and specificity of uptake in lung epithelia. Depending on the therapeutic application, this uptake can often be non-specific and occur in non-desired cell types. Due to this potential non-specificity, these components are often used in combination with one another, are chemically modified, or include targeting ligands or moieties such as peptides, proteins, or antibodies.[6,51]

To improve intracellular uptake into lung epithelia, phage display can be useful for selecting targeting ligands with affinity for cells and specific tissues. We previously used T7 phage combinatorial libraries against a CF-like mucus model and screened for peptides that showed enhanced transport through CF-patient-derived sputum.[19] While this initial work demonstrated that peptides could be used as coatings to improve transport through mucus models, there remained critical questions to address. With this previous screening strategy, while we successfully identified mucus-penetrating peptides, we did not

pan for ligands that can both facilitate mucus penetration and mediate uptake into the CF-affected airway epithelial cells; both barriers are critical bottlenecks to achieving the nucleic acid delivery required for gene therapy. Also, our previous screening was against CF-like mucus with components to best mimic CF clinical samples; however, recent advancements have shown that primary cells isolated from CF patients and grown under appropriate conditions (i.e., ALI) are more accurate physiological models of the disease.[52] As a result, we built upon our previous work and used primary cells derived from CF patients as our selection model. Here, we used fully differentiated primary cells homozygous for the deltaF508 mutation to better reflect this disease state in the human lung. At the ALI, these clinically obtained cells can produce mucus, ciliate, and even mimic CF pathology more closely than traditionally used cell lines.[53–59]

To ensure that candidate ligands facilitated intracellular uptake, we modified our panning strategy to collect peptide-presenting phage internalized by fully differentiated CF epithelia (Figure 1). This approach is in contrast to others' phage display work that primarily focused on collecting and isolating cell surface bound phage on either undifferentiated pHBECs or human bronchial epithelial cell lines.[14,16,60] With our collection method, we increased the probability that only internalized peptide-presenting phage were enriched prior to subsequent rounds in the selection process (Figure 1). Compared to our earlier work,[19] we also greatly modified our panning to increase selection pressure at various rounds (Figure 1B); during selection, the increase in stringency (either by reducing the incubation time and/or increasing washes) should allow selection of the "winners" that can survive in each replicate. In other words, we improved the probability of discovering peptides with increased propensity to get into mucus-producing cells.[61] This enrichment of peptide-presenting phage reflects affinity-based selection, as indicated by other groups.[8,61,62] In our study, after five rounds of selection, we observed a 380-fold enrichment (Figure 1), which aligns with our previous studies that utilized similar T7 phage libraries.[19,21]

Next, we sought to characterize the physicochemical properties of these enriched peptides. We found that sequences present in the fifth round of selection were more positively charged and hydrophilic than those in the first round (Figures 2A and 2B). We measured how hydrophobic or hydrophilic each peptide sequence was using a GRAVY score which, depending on the amino acid composition, can range from −4.5 (most hydrophilic) to 4.5 (most hydrophobic) (Table 1). We observed this shift in hydrophilicity in our previously published work, which supports other findings that suggest hydrophilicity aids in mucus diffusion.[19,63] Additionally, this result corroborates extensive work by others showing that PEG polymer is an attractive coating to improve mucus penetration of carriers due to its hydrophilicity.[6,64–70] For example, Schneider et al. showed that PEGylated nanoparticles have higher mucus diffusion in CF sputum *ex vivo* and more uniform distribution in mouse airway epithelia compared to non-PEGylated nanoparticles.[68] Peptide C, specifically, had a GRAVY score of −1.2, indicating that its sequence is hydrophilic. Furthermore, we saw a trend toward more positively charged peptide sequences from the first to fifth round of selection (Figure 2B). Previously, when we screened against CF-like mucus only, we observed peptide sequences that were more negatively to neutrally net-charged.[19] One potential and likely explanation for this observed difference is that our enriched peptides mimicked more cell-penetrating peptides, which are positively charged in nature, in order to bind and be internalized by cells.[7,71,72] Importantly, we observed that our sequences do not possess a high enough positive charge such that the binding would be too strong with the net negatively charged mucus microenvironment and be stuck for hindered transport.[19,73] For instance, our recent work demonstrated that peptides with a net charge of 5 (at pH 7) have hindered diffusion through CF sputum.[19] This outcome supports work regarding other net negatively charged extracellular environments such as cartilage extracellular matrix in which a highly positively charged peptide would be immobilized.[74] Given that the net charge of our lead peptide candidate is around 2.9, it is probable that the charge is positive enough to allow for weak partitioning through the mucus and subsequent transfection in cells.[73,75] However, others have shown that net charge alone is not sufficient to determine transport and that spatial configuration and sequence order of amino acids also contributes to transport through the mucus barrier.[73] Future studies are warranted to investigate how sequence specificity affects mucus penetration and cellular uptake and how this compares with existing peptides used for pulmonary delivery (both rationally designed and discovered through phage display).

For validation studies, we proceeded with six peptide-displaying phage clones that we identified in the top ten most abundant peptide sequences and in all three replicates after the final round of selection (Table 1). For each of these selected sequences, there was an increased affinity for pHBECs as observed by an increased frequency of the individual clones present in each subsequent round of selection (Figure 3A). This enrichment indicated to us that there was an "evolutionary" pressure to select, and not just screen, for peptides with desired properties for mucus penetration and cell uptake.[61] Additionally, we saw that all peptide-presenting phage clones selected for validation performed better, i.e., achieved greater cellular uptake, compared to a peptide-less control, the original and unselected naive library, and previously discovered mucus-penetrating peptide-presenting phage (i.e., CPS), which further confirmed the improvement in our selection process (Figure 3B). Here, the only difference between all phage clones was the peptide sequence (or lack of it) present on the phage surface. Given this detail, we expect these differences in uptake are based solely on capsid surface properties, which is supported by our other related work.[19,21]

After demonstrating the efficacy of our peptide displayed on the phage capsid, we ultimately wanted to use our targeting peptide ligands to aid gene delivery across mucus and cell barriers. Therefore, we also confirmed that our leading peptide candidate demonstrated similar efficacy when introduced onto a synthetic carrier. Here, we incorporated our peptide, conjugated to a fatty acid tail, into a clinically relevant LNP system as a fifth component. Here, we used

Moderna's Spikevax COVID-19 mRNA vaccine formulation as our base formulation, loaded with NLuc mRNA (Table 2). Cheng et al. demonstrated that a fifth component lipid can be used to supplement LNPs (which typically consist of four lipid components) and, interestingly, depending on the physicochemical property of the lipid, facilitate targeting to specific organs (i.e., lung, liver, spleen) upon systemic delivery.[76] Additionally, others have incorporated peptides in nanoparticle or nanocomplex formulations in order to improve transfection or gene delivery to certain cell types.[70,77–83] Notably, some groups have demonstrated that tandem peptides (i.e., peptides attached to lipid tails) containing targeting peptides can enhance transfection to neuronal, retinal, and cancerous cell lines.[77–79,81,83] In these studies, tandem peptides were complexed or self-assembled with both RNA and protein cargos. For our work, we decided to leverage these advancements by integrating peptides conjugated to myristic acid (14-carbon fatty acid) into LNPs with standard microfluidic mixing.[78,79,83] Here, we confirmed that our Peptide C-lipid could be co-formulated with a conventional four-component LNP and produce LNPs that have acceptable size (diameter <100 nm), are monodisperse (polydispersity index <0.2), and have high encapsulation efficiency (>95%) (Figures 4A and S2).[27] A shift in the zeta-potential measurements toward a more positive value suggests that Peptide C may be partly distributed on the outer surface of the LNP (Figure 4). However, additional work to study structural changes imposed by our Peptide C-lipid conjugate using small-angle X-ray scattering and cryo-TEM are warranted. To validate whether incorporation of our peptide into LNPs could improve transfection and enhance NLuc production, we evaluated LNP transfection using differentiated pHBECs and measured luminescence. After a 48-h incubation period, we observed 10.5-fold and 4.5-fold increased luminescence from mRNA delivered by our Peptide C-LNP compared to LNPs containing additional PEG or a CPS-conjugated lipid, respectively, which were included as mucus-penetrating LNP controls (Figure 4B). These results supported others' findings that the addition of polymers used only for mucus penetration may not be sufficient for also overcoming the cellular barrier.[6] For example, Conte et al. tested and compared PEGylated and non-PEGylated nanoparticles as small interfering RNA carriers for CF treatment. They found that while PEGylated nanoparticles had improved transport through an artificial mucus model, they resulted in lower cellular uptake in a Calu-3 ALI cell model.[6] Additionally, the overall higher NLuc bioactivity for Peptide C- versus Spikevax-LNP-treated cells across various individual CF donors signaled to us that this enhanced bioactivity can be maintained between patients (Figure S3). Given the high inter-patient variability commonly seen in clinically derived samples, these results highlight the attractiveness of this formulation to be effective across different patients. Lastly, the inter-donor variability we observed further highlighted the importance of us using pooled donors for our initial selection strategy.

Nucleic acid delivery to the lungs is not only limited by mucus and cell barriers, but immune cells also present in the airways, especially in diseased lungs.[84,85] Immune cells such as macrophages are present for immunosurveillance during homeostasis, and in CF sputum they can be present in larger numbers compared to a healthy patient.[86,87] Given immune cell presence in the lungs, we sought to determine whether our peptides were selective toward targeted transfection to CF patient epithelia by repeating the same Nano-Glo assay with a THP-1-derived human macrophage cell line. In the previous pHBEC transfection experiment, we hypothesized that if Peptide C-LNPs were more selective for epithelia, we should observe higher mRNA bioactivity compared to all controls. Conversely, in an alternative cell model (i.e., THP-1-derived macrophages), we would expect our Peptide C-LNP-treated cells to exhibit lower or similar bioactivity levels versus other controls. In THP-1 cells, we observed lower luciferase activity from Peptide C-LNP relative to Spikevax and CPS-LNP formulations (Figure 4C). Considering that Peptide C-LNP achieved substantially higher mRNA delivery than other LNPs in pHBECs from CF patients, these results suggest that Peptide C has enhanced transfection in pHBECs relative to the Spikevax "peptide-less" control, compared to macrophages. This result is significant, since inhaled nanoparticles, (e.g., gold nanoparticles) can be cleared by macrophages that reside in the lung.[88–91]

While we have demonstrated that our peptide-LNPs can achieve targeted mRNA delivery in a relevant *in vitro* airway epithelia model of CF, we next wanted to investigate delivery in preclinical models that can better provide the dynamics, anatomical structure, and physiology of the lungs. Here, we delivered LNPs intratracheally to the airways of BALB/c mice to determine whether our leading peptide candidate could enhance delivery of NLuc and subsequent luciferase activity *in vivo*. At 24 h after delivery of LNPs encapsulating NLuc mRNA, we observed significantly higher luminescence compared to all other groups (Figures 5A and 5B). Interestingly, this trend paralleled what we observed *in vitro* using differentiated pHBECs, where luminescence was highest for Peptide C-LNP followed by CPS-LNP, Spikevax, and lastly PEG-LNP-treated mice (Figure 5B). Additionally, since we incorporated a peptide that could cross both mucus and cell barriers, we wanted to ensure that Peptide C did not also influence uptake into other organs non-specifically. In a biodistribution study, we found that mRNA bioactivity remained localized in the lungs following IT delivery, which signaled to us that the risk of systemic exposure is reduced (Figure S4). Recently, multiple groups have used NLuc (and modified NLuc) mRNA to optimize LNP formulations, even for respiratory delivery.[49,92–96] For instance, Lokugamage and colleagues optimized LNPs for nebulization using a modified NLuc reporter gene and demonstrated that their lead LNP could successfully deliver therapeutic mRNA as well. This highlighted that it is possible to replace NLuc reporter mRNA with more clinically relevant cargo and still produce significant results.

We further explored whether Peptide C-LNPs could deliver gene-editing mRNA to lung epithelia *in vivo* using a tdTomato reporter mouse model. In this genetically engineered strain, its DNA includes two *LoxP* stop cassettes that flank and prevent high expression of the tdTomato gene. After delivery and uptake into the nucleus of the cell, Cre recombinase enzyme can excise these DNA stop cassettes, leading to enhanced tdTomato fluorescent protein expression. With this in

mind, we delivered Cre mRNA intratracheally to mouse lungs *in vivo* to determine and quantify which cell types Peptide C-LNPs can edit and to confirm that its uptake in non-desired cell types (i.e., immune cells, endothelia) is comparable to that of PBS-treated mice. We found that our formulation demonstrated significantly higher tdTomato expression in epithelia versus that of immune cells and endothelia (Figure 5D). Coupled with our tissue biodistribution results, this preferential uptake in epithelia is valuable since current lung-targeted therapies that are delivered systemically tend to also have notable uptake in non-epithelia cell types.[45,76,97] Reduced uptake in endothelia can be favorable for avoiding systemic exposure following delivery. Notably, we also found that the percentage of edited epithelia is within values known to restore CFTR function, which may translate favorably when we incorporate therapeutic cargo.[98–100] We would like to note that while this reporter mouse strain is useful for identifying edited cell types, it lacks the mucus microenvironment found in CF lungs, which we aim to explore further. Overall, our *in vivo* results encourage us to exchange our NLuc or Cre mRNA cargo with therapeutic mRNA in future work.

While inclusion of our peptide is a promising first step toward targeted delivery for gene therapy of CF, other important considerations for a clinically relevant product include safety and toxicity profiles of our peptide-LNP formulation. However, initial studies demonstrate that cell viability remains similar between PBS- and Peptide C-LNP-treated mice *in vivo* (Figure S5). Additionally, given that we intratracheally instilled our formulation into mouse lungs, we will need to optimize and formulate these LNPs as stable aerosols for inhalation therapy. Lastly, while we demonstrated that our peptide delivers mRNA to fully differentiated pHBECs *in vitro* and to epithelia *in vivo*, we do not have *a priori* knowledge of the specific epithelial target. The respiratory epithelia contain multiple cell types such as ciliated, goblet, basal, and ionocyte cells, some of which are thought to play a prominent role in CFTR expression, hinting that therapy should be directed to these cell types.[45,101–103] While our panning allowed for unbiased identification of peptide ligands against cells, it would be important to understand which specific cell type is targeted and elucidate the mechanism of how these peptides achieve delivery. With these goals in mind, our peptide discovered through phage display and stringent selection demonstrates significant progress given that it can successfully target differentiated pHBECs and even enhance transfection *in vivo*. It is also important to note that since the formulations were based on the components of the COVID-19 mRNA vaccine and used a similar formulation strategy, i.e., nanoprecipitation by microfluidic mixing, our targeting approach can be easily formulated and scaled up to clinical use.

In this work, we implemented an improved phage display selection strategy and discovered a lead peptide that significantly enhanced mRNA bioactivity to fully differentiated pHBECs from CF patients and to mouse airways *in vivo*. Given that we successfully and easily implemented our peptide as a fifth component to traditional LNPs, we anticipate these peptide-LNPs could deliver more clinically relevant nucleic acids for CF therapy (e.g., CRISPR-Cas9-editing mRNA). Further, we conducted this work with an FDA-approved LNP formulation, which demonstrates the clinical relevance of our LNP formulation. In future studies, we anticipate that our peptide could be added to other LNP systems that have been specifically optimized for pulmonary delivery. While gene therapy for CF has been a significant challenge due to poor delivery efficacy to the lungs, we are encouraged by our results presented here and see potential for our mucus- and cell-penetrating targeting peptide to overcome this delivery barrier.

MATERIALS AND METHODS

Differentiation of primary human bronchial epithelial cells

For coating Transwell® inserts (0.4 μm, 6.5 mm diameter, Corning Product, catalog #3470), we prepared Human Placenta Collagen Type IV (Sigma, catalog #C7521) according to protocols established by University of North Carolina, Marisco Lung Institute (MLI) core. We first prepared a 10× stock solution (10 mg of collagen, 20 mL of ddH_2O, 50 μL of concentrated acetic acid) and incubated from 4 to 8 h at 37°C to dissolve. We then filter sterilized the solution with a 0.2-μm syringe filter, aliquoted, and stored at −20°C. Prior to coating, we prepared a 1× solution with sterile cell culture grade water. Next, we added 100 μL to each insert, dried plates containing inserts (with lids off) in a biosafety cabinet overnight, and UV sterilized inserts for at least 30 min before use.

From MLI, we purchased primary human bronchial epithelial cells (pHBECs) from seven different cystic fibrosis (CF) patients homozygous for the deltaF508 mutation (for patient demographics see Table S1). All cells used for experiments were passage 2 (P2) unless otherwise noted. We seeded either pooled (all seven CF patients) or individual CF donors onto precoated inserts for differentiation at ALI according to Pneumacult Ex-Plus (STEMCELL Technologies, Vancouver, Canada, catalog #05040; supplemented with amphotericin B [0.25 μg/mL final concentration; Thermo Fisher Scientific, catalog #BP264520], gentamicin [50 μg/mL final concentration; Sigma, catalog #G1397], and 1× penicillin/streptomycin) and Pneumacult-ALI medium (STEMCELL Technologies, catalog #05001; supplemented with 1× penicillin/streptomycin) protocols. In brief, we first expanded P2 cells on precoated Transwell® inserts until at least 80% confluence. Once confluence was reached, we removed apical medium (i.e., airlifted cells), and added Pneumacult-ALI maintenance medium to the basolateral side only. We then maintained cells in Pneumacult-ALI maintenance medium until differentiation occurred (at least 21 days post airlift and confirmed by observation with mucus production and cilia movement). Prior to selection studies, we briefly washed cells 2 and 3 weeks post airlift and 1 day prior to the first round of selection. For washes, we incubated cells with 200 μL of Dulbecco's PBS (DPBS) (without Ca^{2+} and Mg^{2+}) for 30 min at 37°C.

Differentiation of THP-1 cells for macrophage transfection studies

For macrophage transfection studies, we cultured THP-1 cells (ATCC, catalog #TIB-202) according to ATCC's recommendations. In brief, we maintained cells in RPMI-1640 medium (Sigma,

catalog #R8758) supplemented with 10% fetal bovine serum (FBS) and gentamicin (final concentration of 50 μg/mL). For differentiation into non-polarized macrophages, we resuspended cells in phorbol 12-myristate 13-acetate (PMA) (Sigma, catalog #P8139) containing medium (15 ng/mL) and seeded at a final density of 4×10^5 viable cells/mL. We seeded 0.5 mL of cell suspension per well for a 24-well plate. We incubated cells at 37°C/5% CO_2 for 48 h before exchanging medium with PMA-free medium and incubating cells for an additional 24 h prior to use for experiments.

Selection strategy

We used T7 CX_7C phage libraries previously made in our lab[19,21] using the T7Select415-1 cloning kit (Novagen, catalog #70015) to select against CF pHBECs pooled from seven different CF donors to discover mucus and cell-penetrating peptides. We combined T7 libraries and diluted them in DPBS (without Ca^{2+} and Mg^{2+}) to a final concentration of 3.3×10^5 plaque-forming units (PFU)/μL to obtain 1,000 viral genomes per cell (we seeded 3.3×10^4 pHBECs per insert). One day prior to the first round of selection, excess mucus was removed. We then added 100 μL of phage solution to the apical side of each Transwell® insert (n = 3) and incubated for a given amount of time depending on the round of selection (round 1 = 16 h, round 2 = 4 h, rounds 3–5 = 1 h). We chose a longer time point in the first round of selection to allow for a higher yield of phage for subsequent rounds and increased stringency in the following rounds by shortening the incubation time down to 1 h by the final round.[8,9,11,104] Previous research has shown that a significant portion of aerosolized particles can remain in the lungs of CF patients for up to 60 min,[105,106] so we determined 1 h to be well within potential clearance times for CF patients. Additionally, similar time points have been successful in previous directed evolution studies for the enrichment of lung-targeting adeno-associated viruses.[8,9] Importantly, we also did not perform any mucus washes at the start of the selection process to allow for the buildup of mucus for each subsequent round. After incubation, we removed apical and basolateral solutions and washed cells with phage elution buffer (20 mM Tris-HCl [pH 8], 100 mM NaCl, 6 mM $MgSO_4$) and DPBS to remove any unbound/bound phage remaining. After wash steps, we added 200 μL of M-PER lysis buffer (Thermo Fisher Scientific, catalog #78503) on top of cells and incubated for 5 min at 180 rpm on an orbital shaker to ensure cell lysis. Following lysis, we scraped cells (using a P200 pipette tip), collected lysate, and spun cells down for 10 min at 14,000 × g to separate cell debris from internalized phage (present in supernatant). We then quantified and titered collected phage using a standard double-layer plaque assay. After each round, we pooled internalized phage from each replicate and used this pool as input for the following round. We believe this additional optimization step improved reproducibility in our selection process compared to our previous screening strategy, where we had few clones present in all three replicates.[19] Additionally, after sample collection, we reserved a portion of this sample for NGS and amplified the remaining sample in *E. coli* (BL21) until lysis was observed (∼2 h) as per manufacturer's protocol, so input concentrations remained the same in the following rounds. As a control to identify parasitic sequences,[107] the naive library (unselected CX_7C library) was amplified five subsequent times prior to NGS sample preparation.

To ensure that the volume administered during our fifth round of selection did not remove the mucus layer on top of pHBECs, we administered 100 μL of DPBS on top of fully differentiated pHBECs and incubated cells for 1 h, rinsed wells twice with 150 μL of DPBS, and stained mucus with 100 μL of Alcian blue 8GX (Sigma-Aldrich, catalog #66011) for 15 min at room temperature. After staining, we rinsed cells three times with 200 μL of DPBS and imaged at 4× magnification. Treated cells were compared to poorly differentiated cells (to serve as a low mucus control) and untreated differentiated pHBECs.

Next-generation sequencing data analysis

Following each round of selection, we isolated DNA from amplified phage, prepared samples for NGS and performed peptide sequence analysis as previously reported.[19,21] After obtaining a frequency count of all peptide sequences from each round of panning and in order to properly select enriched CX_7C sequences from our NGS data, we omitted sequences that were linear (i.e., did not contain the expected CX_7C motif) or did not contain the correct flanking sequences surrounding the insert initially cloned into our library. We then analyzed the top 30 most abundant sequences after all five rounds of selection to determine their physicochemical properties. Specifically, we calculated net charge and grand average of hydropathy score (GRAVY score) for each 7-mer sequence using *in silico* tools (https://pepcalc.com and http://www.gravy-calculator.de/index.php, respectively). Additionally, we created a multiple-sequence-alignment visual representation using Seq2Logo after we combined the top 30 sequences from each replicate (total of 90 sequences) after five rounds of selection.[22] Peptide sequences that were present in the top ten most frequently occurring peptide sequences in all three replicates and were absent from an amplified naive library control (amplified five times to correlate with the five rounds of panning) were selected for further validation studies. We evaluated the enrichment for each clone selected for validation studies by calculating the average (n = 3) percentage of total unique sequences retrieved from NGS for each round of selection. Additionally, we analyzed peptide sequences using the online tool SAROTUP to confirm that sequences used for validation were not target-unrelated peptides.[24–26]

Validation of clones

After we selected peptides from NGS data for further validation, we cloned these peptide sequences back into T7 phage and verified them through Sanger sequencing as previously published.[21] In brief, we obtained complementary pairs of oligonucleotides (i.e., sense and anti-sense oligos) for each peptide sequence through IDT (Table S2). Oligos were diluted in IDTE buffer, pH 8 (IDT, catalog #11-01-02-05) to a 100-μM stock solution and then to 10-μM working solution before use. We then annealed oligos (5 μL of 10 μM sense and anti-sense oligos in a 50-μL reaction) with ultrapure water

at 95°C for 3 min before cooling to room temperature (25°C) at 0.1°C/s (ramp). After annealing, inserts were ligated to T7-Select 415-1 vector arms (Novagen [EMD Millipore], catalog #70015-3) using T4 DNA ligase (New England Biolabs, catalog #M0202L). We then packaged ligation reactions using T7Select415-1b cloning kit (Novagen [EMD Millipore], catalog #70015-3) according to the manufacturer's instructions. We plated packaged clones using a standard double-layer plaque assay with BL21 *E. coli*. After incubating clones overnight at 37°C, we isolated and sequenced individual plaques to confirm proper cloning. Once clones were validated, they were amplified in liquid BL21 *E. coli* culture prior to validation studies. To validate clones for enhanced CF pHBEC transfection, we incubated 3.3×10^7 PFU of each clone (in 100 μL of DPBS) on the apical side of differentiated pHBECs for 1 h at 37°C. Phage were collected and quantified in the same manner as our selection for round 5.

In vitro transcription

We prepared nanoluciferase mRNA (NLuc) as previously published.[49] In brief, we created a template for NLuc mRNA encoding sequences for a T7 promoter, 5′ UTR, codon-optimized NLuc, and 3′ UTR. We synthesized mRNA using the AmpliScribe T7-Flash Transcription Kit (Lucigen, catalog #ASF-3507) as described previously.[108,109] After purification with RNA Clean & Concentrator-100 (Zymo, catalog #R1019), we added a cap1 structure using the Vaccinia Capping System (NEB, catalog #M2080S) and mRNA Cap 2′-*O*-methyltransferase (NEB, catalog #M0366S). We then added a 3′-poly(A) tail (E. Coli Poly(A) Polymerase; NEB, catalog #M0276L). After polyadenylation, we purified mRNA again and determined mRNA concentration by NanoDrop 1000 (Thermo Fisher Scientific) and stored aliquots at −80°C until use.

Lipid nanoparticle synthesis

To determine whether peptides discovered through phage display could be incorporated into a nanoparticle system, we used cyclic peptides conjugated to a myristic acid lipid tail (synthesized and N-terminally modified by LifeTein). We used this peptide-lipid as a fifth component to Moderna's Spikevax lipid nanoparticle formulation using a NanoAssemblr Benchtop instrument (Precision Nanosystems, Vancouver, BC, Canada). In brief, lipids (peptide-lipid, SM-102 [Echelon, catalog #*N*-1102], cholesterol [Sigma, catalog #C8667], distearoylphosphatidylcholine [DSPC] [Avanti, catalog #850365], and 1,2-dimyristoyl-rac-glycero-3-methoxypolyethylene [DMG-PEG] [Avanti, catalog #880151P]) were dissolved in molecular-grade ethanol at a concentration of 10 mg/mL, and reporter mRNA (NLuc) was dissolved in prechilled sodium citrate buffer (pH 4, 100 mM). We prepared formulations via microfluidic mixing using a Y-shaped staggered herringbone mixer[27] at an aqueous/organic flow ratio of 3:1, flow rate of 4 mL/min, and volume of 500–1,000 μL. After formulation, LNPs were dialyzed in 1× PBS (pH 7.4) for 2 h (for *in vitro* experiments) or at least 4 h (for *in vivo* experiments) in 10K molecular-weight-cutoff Slide-A-Lyzer dialysis cassettes (Thermo Fisher Scientific, catalog #87730).

Lipid nanoparticle characterization

For characterization, we prepared LNPs in 1× PBS (pH 7.4) for size measurements (10-fold dilution) by DLS and in ultra-pure water for zeta potential measurements (40-fold dilution) using Zetasizer Nano-ZS (Malvern Instruments, MA, USA). To determine encapsulation efficiency percentages (EE%), we used a modified Quant-it RiboGreen RNA Assay Kit protocol (Thermo Fisher Scientific, catalog #R11490). In brief, LNPs were diluted 100-fold in 1× Tris-EDTA (TE) or 1% Triton X-100 (Thermo Fisher Scientific, catalog #BP151) to measure unencapsulated mRNA or total mRNA, respectively. We additionally prepared two low-range standard curves (one in TE and one in 1% Triton X-100). We added 100 μL of LNP sample or standard to a clear-bottom 96-well black plate (Corning, catalog #3631) in duplicate, then proceeded to incubate all samples and standards at 37°C for 10 min. We then added a 2,000-fold dilution of RiboGreen Reagent and added 100 μL of the working solution to each sample or standard. After 5 min, we measured fluorescence using a SpectraMax M3 plate reader (Molecular Devices) at excitation/emission of 480 nm/520 nm. We calculated EE% by the following equation: $[1 - (\text{unencapsulated mRNA/total mRNA})] \times 100$.

For TEM characterization, we added 5 μL of LNP formulation (55 ng/μL) onto a carbon support film (Ted Pella, catalog #01820), incubated for 1 min, and briefly rinsed with water. Directly after rinsing, we briefly stained with 2% uranyl acetate (up to 3 s), blotted excess stain, and let dry overnight. Images were taken at 50× magnification at 200 kV using the JEOL NEOARM (Texas Materials Institute).

Lipid nanoparticle transfection *in vitro*

To compare transfection of our LNP formulations, we incubated either differentiated CF pHBECs (pooled from seven individual CF donors) or THP-1-derived macrophages with 450 ng of mRNA (based on EE% values) for 48 h. For initial validation studies, we diluted LNPs in 1× PBS to 3.6 ng of NLuc mRNA/μL for a total dosing volume of 125 μL. We measured NLuc bioactivity by bioluminescence assay using Nano-Glo Luciferase Assay System (Promega [Madison, WI], catalog #N1110). In brief, for pHBECs, we scraped cells from each treated well (remaining LNP solution left on top) and transferred to a 96-well white flat-bottom plate (Corning, catalog #3912). For differentiated THP-1 cells we removed medium first, then added 50 μL of 1× PBS (without Ca^{2+} or Mg^{2+}) to cells before scraping and collecting (to keep apical volume consistent with pHBECs). We incubated collected samples with a 1:1 ratio of Nano-Glo Luciferase Assay Buffer to lyse the cells. Nano-Glo substrate was added to each well (one group at a time), and luminescence was read 3 min later using a SpectraMax M3 plate reader (Molecular Devices).

To compare transfection of our LNP formulations on individual donors, we diluted LNPs in 1× PBS to 6 ng of NLuc mRNA/μL and incubated pHBECs ($n = 4$) with 75 μL (450 ng) of mRNA (based on formulation concentration) for 48 h. We first removed medium and remaining LNP solution, then added 50 μL of 1× PBS (without Ca^{2+} or Mg^{2+}) to cells before scraping and collecting before

measuring bioluminescence in similar manner to measurements on pooled pHBECs and THP-1-derived macrophages using the BioTek Synergy H1 Multimode Reader (Agilent).

Lipid nanoparticle delivery *in vivo*

We performed all procedures in accordance with and under approval and oversight by the University of Texas at Austin Institutional Animal Care and Use Committee. For intratracheal administration, we first anesthetized BALB/c mice (Charles River, female, 6–8 weeks old) under 2% isoflurane before delivering 40 μL of each LNP formulation in two separate instillations of 20 μL. Twenty-four hours after administration of LNPs, we euthanized mice via carbon dioxide inhalation followed by cervical dislocation and immediately harvested lungs. We briefly rinsed harvested lungs by dipping in 1× PBS and separated each lung into five separate lobes (left, cranial, middle, accessory, and caudal). We then collected lobes for each lung into a 1.5-mL microcentrifuge tube and incubated in 300 μL of Nano-Glo substrate solution for 5 min before proceeding directly to imaging using an IVIS Spectrum *in vivo* imaging system (Xenogen, Alameda, CA). We measured bioluminescence (average radiance [p/s/cm^2/sr] calculated for area surrounding all five lobes) using Living Image 4.3 software (PerkinElmer, Waltham, MA).

For biodistribution studies, we dosed BALB/c mice (Charles River, female) with either Peptide C-LNPs or PBS as stated above, harvested organs (brain, heart, lung, liver, spleen, kidneys, and GI tract), then briefly rinsed each organ by dipping in 1× PBS prior to collecting all organs (except brain) in a 15-mL conical tube. Due to the delicate nature of the brain, we collected this organ in a separate 15-mL conical tube. For each mouse, once we collected all organs we incubated the heart, lungs, liver, spleen, kidneys, and GI tract in 3 mL of Nano-Glo substrate solution and the brain in 1 mL of the same substrate solution. We incubated organs for 10 min with gentle agitation throughout the incubation period, prior to imaging by IVIS as stated previously.

For intratracheal administration of Cre mRNA, we first anesthetized Ai9 mice (The Jackson Laboratory, catalog #007909) under 2% isoflurane before delivering 50 μL of either 1× PBS or Peptide C-LNP formulation (0.5 mg/kg of Cre recombinase mRNA) (TriLink catalog #L7211) in two separate instillations of 25 μL. Seventy-two hours after administration, we euthanized mice via carbon dioxide inhalation followed by cervical dislocation and immediately harvested the lungs. We briefly rinsed harvested lungs by dipping in 1× PBS. To determine *in vivo* gene editing following local administration of our Peptide C-LNPs, we processed the harvested lungs for flow cytometry as described previously.[49,110] In brief, we digested lungs in 10 mL of digestion medium (90 units/mL collagenase type I [Sigma, catalog #SCR103], 50 units/mL DNase I [Roche, catalog #11284932001], 60 units/mL hyaluronidase [Sigma, catalog #H3506]) for 1 h at 37°C with intermittent shaking. We formed a single-cell suspension by pouring the digested contents over a 70-μm filter and quenched digestion with 10 mL of wash buffer (DMEM, 20% FBS, and 1% penicillin/streptomycin). We centrifuged the quenched solution at 300 × *g* for 10 min at 4°C, washed cells with 5 mL of 1× PBS, and lysed red blood cells by incubating cells in 5 mL of ACK lysing buffer (Thermo Fisher Scientific, catalog #A10492-01) at room temperature for 3 min, prior to quenching with 10 mL of quench buffer (90% 1× PBS, 10% FBS). We washed cells with wash buffer followed by an additional PBS wash and resuspended cells in 1× PBS prior to staining for flow cytometry as previously described.[49] For staining we used the following antibodies and viability dye: immune cells (CD45-Pacific Blue, BioLegend, catalog #103126), endothelial cells (CD31-AF488, BioLegend, catalog #102414), epithelial cells (CD326-AF647, BioLegend, catalog #118212), and viability dye (Zombie NIR, BioLegend, catalog #77184). We performed flow cytometry and analysis using the Attune NxT Acoustic Focusing Cytometer (Thermo Fisher Scientific) and FlowJo 10.10.0 software.

Statistical analysis

We performed all data analyses with GraphPad Prism 10 (GraphPad Software, La Jolla, CA) at a significance level of $p \leq 0.05$ unless otherwise indicated.

DATA AND CODE AVAILABILITY

The data for this study can be made available from the corresponding author upon reasonable request.

ACKNOWLEDGMENTS

We would like to especially acknowledge Leslie Fulcher, Dr. Scott Randell, and the Marisco Lung Institute/Cystic Fibrosis and Pulmonary Disease Research and Treatment Center at the University of North Carolina at Chapel-Hill for providing the primary cells used in this study. Additionally, we would like to extend our biggest thanks to Xiujuan (Sophie) Peng and Tony Dong for providing the CX_7C libraries. Lastly, we would like to acknowledge UT's Center for Biomedical Research Support and Dr. Xun Zhan at the Texas Materials Institute for their assistance in acquiring NGS data and TEM images, respectively. This work was supported by the Cystic Fibrosis Foundation (GHOSH19XX0 and LEAL19XX0) and by the National Institutes of Health (R01 HL138251 and R01 HL138251S1).

AUTHOR CONTRIBUTIONS

M.R.S., D.G., and J.L. participated in the study conceptualization. M.R.S., M.M.L., J.L., and R.P.M. took part in the methodology. M.R.S., M.M.L., Y.P., A.V., B.J.H., and E.Y.M. participated in the investigation process. M.R.S. and D.G. wrote the original draft, and M.R.S., D.G., M.M.L., Y.P., R.P.M., J.L., A.V., B.J.H., and E.Y.M. contributed to reviewing and editing the final draft of the manuscript.

DECLARATION OF INTERESTS

This research has a patent application by the University of Texas at Austin.

SUPPLEMENTAL INFORMATION

Supplemental information can be found online at https://doi.org/10.1016/j.omtn.2024.102375.

REFERENCES

1. Yeung, J.C., Machuca, T.N., Chaparro, C., Cypel, M., Stephenson, A.L., Solomon, M., Saito, T., Binnie, M., Chow, C.W., Grasemann, H., et al. (2020). Lung transplantation for cystic fibrosis. J. Heart Lung Transplant. *39*, 553–560. https://doi.org/10.1016/j.healun.2020.02.010.

2. Turcios, N.L. (2020). Cystic Fibrosis Lung Disease: An Overview. Respir. Care *65*, 233–251. https://doi.org/10.4187/respcare.06697.

3. McLachlan, G., Alton, E.W.F.W., Boyd, A.C., Clarke, N.K., Davies, J.C., Gill, D.R., Griesenbach, U., Hickmott, J.W., Hyde, S.C., Miah, K.M., and Molina, C.J. (2022).

Progress in Respiratory Gene Therapy. Hum. Gene Ther. *33*, 893–912. https://doi.org/10.1089/hum.2022.172.

4. Shirley, J.L., de Jong, Y.P., Terhorst, C., and Herzog, R.W. (2020). Immune Responses to Viral Gene Therapy Vectors. Mol. Ther. *28*, 709–722. https://doi.org/10.1016/j.ymthe.2020.01.001.

5. Bulcha, J.T., Wang, Y., Ma, H., Tai, P.W.L., and Gao, G. (2021). Viral vector platforms within the gene therapy landscape. Signal Transduct. Targeted Ther. *6*, 53. https://doi.org/10.1038/s41392-021-00487-6.

6. Conte, G., Costabile, G., Baldassi, D., Rondelli, V., Bassi, R., Colombo, D., Linardos, G., Fiscarelli, E.V., Sorrentino, R., Miro, A., et al. (2022). Hybrid Lipid/Polymer Nanoparticles to Tackle the Cystic Fibrosis Mucus Barrier in siRNA Delivery to the Lungs: Does PEGylation Make the Difference? ACS Appl. Mater. Interfaces *14*, 7565–7578. https://doi.org/10.1021/acsami.1c14975.

7. Ghosh, D., Peng, X., Leal, J., and Mohanty, R. (2018). Peptides as drug delivery vehicles across biological barriers. J. Pharm. Investig. *48*, 89–111. https://doi.org/10.1007/s40005-017-0374-0.

8. Excoffon, K.J.D.A., Koerber, J.T., Dickey, D.D., Murtha, M., Keshavjee, S., Kaspar, B.K., Zabner, J., and Schaffer, D.V. (2009). Directed evolution of adeno-associated virus to an infectious respiratory virus. Proc. Natl. Acad. Sci. USA *106*, 3865–3870. https://doi.org/10.1073/pnas.0813365106.

9. Li, W., Zhang, L., Johnson, J.S., Zhijian, W., Grieger, J.C., Ping-Jie, X., Drouin, L.M., Agbandje-McKenna, M., Pickles, R.J., and Samulski, R.J. (2009). Generation of novel AAV variants by directed evolution for improved CFTR delivery to human ciliated airway epithelium. Mol. Ther. *17*, 2067–2077. https://doi.org/10.1038/mt.2009.155.

10. Sinn, P.L., Hwang, B.Y., Li, N., Ortiz, J.L.S., Shirazi, E., Parekh, K.R., Cooney, A.L., Schaffer, D.V., and McCray, P.B., Jr. (2017). Novel GP64 envelope variants for improved delivery to human airway epithelial cells. Gene Ther. *24*, 674–679. https://doi.org/10.1038/gt.2017.78.

11. Smith, G.P., and Petrenko, V.A. (1997). Phage Display. Chem. Rev. *97*, 391–410. https://doi.org/10.1021/cr960065d.

12. Oyama, T., Sykes, K.F., Samli, K.N., Minna, J.D., Johnston, S.A., and Brown, K.C. (2003). Isolation of lung tumor specific peptides from a random peptide library: generation of diagnostic and cell-targeting reagents. Cancer Lett. *202*, 219–230. https://doi.org/10.1016/j.canlet.2003.08.011.

13. Grant-Serroukh, D., Hunter, M.R., Maeshima, R., Tagalakis, A.D., Aldossary, A.M., Allahham, N., Williams, G.R., Edbrooke, M., Desai, A., and Hart, S.L. (2022). Lipid-peptide nanocomplexes for mRNA delivery in vitro and in vivo. J. Contr. Release *348*, 786–797. https://doi.org/10.1016/j.jconrel.2022.06.018.

14. Romanczuk, H., Galer, C.E., Zabner, J., Barsomian, G., Wadsworth, S.C., and O'Riordan, C.R. (1999). Modification of an adenoviral vector with biologically selected peptides: a novel strategy for gene delivery to cells of choice. Hum. Gene Ther. *10*, 2615–2626. https://doi.org/10.1089/10430349950016654.

15. Ghosh, D., and Barry, M.A. (2005). Selection of muscle-binding peptides from context-specific peptide-presenting phage libraries for adenoviral vector targeting. J. Virol. *79*, 13667–13672. https://doi.org/10.1128/JVI.79.21.13667-13672.2005.

16. Writer, M.J., Marshall, B., Pilkington-Miksa, M.A., Barker, S.E., Jacobsen, M., Kritz, A., Bell, P.C., Lester, D.H., Tabor, A.B., Hailes, H.C., et al. (2004). Targeted gene delivery to human airway epithelial cells with synthetic vectors incorporating novel targeting peptides selected by phage display. J. Drug Target. *12*, 185–193. https://doi.org/10.1080/10611860410001724459.

17. Jost, P.J., Harbottle, R.P., Knight, A., Miller, A.D., Coutelle, C., and Schneider, H. (2001). A novel peptide, THALWHT, for the targeting of human airway epithelia. FEBS Lett. *489*, 263–269. https://doi.org/10.1016/s0014-5793(00)02236-5.

18. Staquicini, D.I., Barbu, E.M., Zemans, R.L., Dray, B.K., Staquicini, F.I., Dogra, P., Cardó-Vila, M., Miranti, C.K., Baze, W.B., Villa, L.L., et al. (2021). Targeted Phage Display-based Pulmonary Vaccination in Mice and Non-human Primates. Méd. *2*, 321–342. https://doi.org/10.1016/j.medj.2020.10.005.

19. Leal, J., Peng, X., Liu, X., Arasappan, D., Wylie, D.C., Schwartz, S.H., Fullmer, J.J., McWilliams, B.C., Smyth, H.D.C., and Ghosh, D. (2020). Peptides as surface coatings of nanoparticles that penetrate human cystic fibrosis sputum and uniformly distribute in vivo following pulmonary delivery. J. Contr. Release *322*, 457–469. https://doi.org/10.1016/j.jconrel.2020.03.032.

20. Fulcher, M.L., Gabriel, S., Burns, K.A., Yankaskas, J.R., and Randell, S.H. (2005). Well-Differentiated Human Airway Epithelial Cell Cultures. In Human Cell Culture Protocols, J. Picot, ed. (Humana Press), pp. 183–206. https://doi.org/10.1385/1-59259-861-7:183.

21. Mohanty, R.P., Liu, X., Kim, J.Y., Peng, X., Bhandari, S., Leal, J., Arasappan, D., Wylie, D.C., Dong, T., and Ghosh, D. (2019). Identification of peptide coatings that enhance diffusive transport of nanoparticles through the tumor microenvironment. Nanoscale *11*, 17664–17681. https://doi.org/10.1039/c9nr05783h.

22. Thomsen, M.C.F., and Nielsen, M. (2012). Seq2Logo: a method for construction and visualization of amino acid binding motifs and sequence profiles including sequence weighting, pseudo counts and two-sided representation of amino acid enrichment and depletion. Nucleic Acids Res. *40*, W281–W287. https://doi.org/10.1093/nar/gks469.

23. Kyte, J., and Doolittle, R.F. (1982). A simple method for displaying the hydropathic character of a protein. J. Mol. Biol. *157*, 105–132. https://doi.org/10.1016/0022-2836(82)90515-0.

24. He, B., Chai, G., Duan, Y., Yan, Z., Qiu, L., Zhang, H., Liu, Z., He, Q., Han, K., Ru, B., et al. (2016). BDB: biopanning data bank. Nucleic Acids Res. *44*, D1127–D1132. https://doi.org/10.1093/nar/gkv1100.

25. Huang, J., Ru, B., Li, S., Lin, H., and Guo, F.B. (2010). SAROTUP: scanner and reporter of target-unrelated peptides. J. Biomed. Biotechnol. *2010*, 101932. https://doi.org/10.1155/2010/101932.

26. Huang, J., Ru, B., Zhu, P., Nie, F., Yang, J., Wang, X., Dai, P., Lin, H., Guo, F.B., and Rao, N. (2012). MimoDB 2.0: a mimotope database and beyond. Nucleic Acids Res. *40*, D271–D277. https://doi.org/10.1093/nar/gkr922.

27. Roces, C.B., Lou, G., Jain, N., Abraham, S., Thomas, A., Halbert, G.W., and Perrie, Y. (2020). Manufacturing Considerations for the Development of Lipid Nanoparticles Using Microfluidics. Pharmaceutics *12*, 1095. https://doi.org/10.3390/pharmaceutics12111095.

28. Madisen, L., Zwingman, T.A., Sunkin, S.M., Oh, S.W., Zariwala, H.A., Gu, H., Ng, L.L., Palmiter, R.D., Hawrylycz, M.J., Jones, A.R., et al. (2010). A robust and high-throughput Cre reporting and characterization system for the whole mouse brain. Nat. Neurosci. *13*, 133–140. https://doi.org/10.1038/nn.2467.

29. Labiris, N.R., and Dolovich, M.B. (2003). Pulmonary drug delivery. Part I: physiological factors affecting therapeutic effectiveness of aerosolized medications. Br. J. Clin. Pharmacol. *56*, 588–599. https://doi.org/10.1046/j.1365-2125.2003.01892.x.

30. Labiris, N.R., and Dolovich, M.B. (2003). Pulmonary drug delivery. Part II: the role of inhalant delivery devices and drug formulations in therapeutic effectiveness of aerosolized medications. Br. J. Clin. Pharmacol. *56*, 600–612. https://doi.org/10.1046/j.1365-2125.2003.01893.x.

31. Patton, J.S., and Byron, P.R. (2007). Inhaling medicines: delivering drugs to the body through the lungs. Nat. Rev. Drug Discov. *6*, 67–74. https://doi.org/10.1038/nrd2153.

32. Williams, D.M. (2018). Clinical Pharmacology of Corticosteroids. Respir. Care *63*, 655–670. https://doi.org/10.4187/respcare.06314.

33. Sadiq, M.W., Holz, O., Ellinghusen, B.D., Faulenbach, C., Müller, M., Badorrek, P., Eriksson, U.G., Fridén, M., Stomilovic, S., Lundqvist, A.J., and Hohlfeld, J.M. (2021). Lung pharmacokinetics of inhaled and systemic drugs: A clinical evaluation. Br. J. Pharmacol. *178*, 4440–4451. https://doi.org/10.1111/bph.15621.

34. Bhat, P.G., Flanagan, D.R., and Donovan, M.D. (1996). Drug diffusion through cystic fibrotic mucus: steady-state permeation, rheologic properties, and glycoprotein morphology. J. Pharmaceut. Sci. *85*, 624–630. https://doi.org/10.1021/js950381s.

35. Wine, J.J. (1999). The genesis of cystic fibrosis lung disease. J. Clin. Invest. *103*, 309–312. https://doi.org/10.1172/JCI6222.

36. Sanders, N.N., De Smedt, S.C., Van Rompaey, E., Simoens, P., De Baets, F., and Demeester, J. (2000). Cystic fibrosis sputum: a barrier to the transport of nanospheres. Am. J. Respir. Crit. Care Med. *162*, 1905–1911. https://doi.org/10.1164/ajrccm.162.5.9909009.

37. Dawson, M., Wirtz, D., and Hanes, J. (2003). Enhanced viscoelasticity of human cystic fibrotic sputum correlates with increasing microheterogeneity in particle transport. J. Biol. Chem. *278*, 50393–50401. https://doi.org/10.1074/jbc.M309026200.

38. Suk, J.S., Lai, S.K., Wang, Y.Y., Ensign, L.M., Zeitlin, P.L., Boyle, M.P., and Hanes, J. (2009). The penetration of fresh undiluted sputum expectorated by cystic fibrosis patients by non-adhesive polymer nanoparticles. Biomaterials *30*, 2591–2597. https://doi.org/10.1016/j.biomaterials.2008.12.076.

39. Kavanagh, E.W., Tzeng, S.Y., Sharma, N., Cutting, G.R., and Green, J.J. (2025). Ligand-free biodegradable poly(beta-amino ester) nanoparticles for targeted systemic delivery of mRNA to the lungs. Biomaterials *313*, 122753. https://doi.org/10.1016/j.biomaterials.2024.122753.

40. Patel, A.K., Kaczmarek, J.C., Bose, S., Kauffman, K.J., Mir, F., Heartlein, M.W., DeRosa, F., Langer, R., and Anderson, D.G. (2019). Inhaled Nanoformulated mRNA Polyplexes for Protein Production in Lung Epithelium. Adv. Mater. *31*, e1805116. https://doi.org/10.1002/adma.201805116.

41. Mastorakos, P., da Silva, A.L., Chisholm, J., Song, E., Choi, W.K., Boyle, M.P., Morales, M.M., Hanes, J., and Suk, J.S. (2015). Highly compacted biodegradable DNA nanoparticles capable of overcoming the mucus barrier for inhaled lung gene therapy. Proc. Natl. Acad. Sci. USA *112*, 8720–8725. https://doi.org/10.1073/pnas.1502281112.

42. Tafech, B., Rokhforouz, M.R., Leung, J., Sung, M.M., Lin, P.J., Sin, D.D., Lauster, D., Block, S., Quon, B.S., Tam, Y., et al. (2024). Exploring Mechanisms of Lipid Nanoparticle-Mucus Interactions in Healthy and Cystic Fibrosis Conditions. Adv. Healthcare Mater. *13*, e2304525. https://doi.org/10.1002/adhm.202304525.

43. Ongun, M., Lokras, A.G., Baghel, S., Shi, Z., Schmidt, S.T., Franzyk, H., Rades, T., Sebastiani, F., Thakur, A., and Foged, C. (2024). Lipid nanoparticles for local delivery of mRNA to the respiratory tract: Effect of PEG-lipid content and administration route. Eur. J. Pharm. Biopharm. *198*, 114266. https://doi.org/10.1016/j.ejpb.2024.114266.

44. Kim, J., Jozic, A., Lin, Y., Eygeris, Y., Bloom, E., Tan, X., Acosta, C., MacDonald, K.D., Welsher, K.D., and Sahay, G. (2022). Engineering Lipid Nanoparticles for Enhanced Intracellular Delivery of mRNA through Inhalation. ACS Nano *16*, 14792–14806. https://doi.org/10.1021/acsnano.2c05647.

45. Sun, Y., Chatterjee, S., Lian, X., Traylor, Z., Sattiraju, S.R., Xiao, Y., Dilliard, S.A., Sung, Y.C., Kim, M., Lee, S.M., et al. (2024). In vivo editing of lung stem cells for durable gene correction in mice. Science *384*, 1196–1202. https://doi.org/10.1126/science.adk9428.

46. Alton, E.W., Stern, M., Farley, R., Jaffe, A., Chadwick, S.L., Phillips, J., Davies, J., Smith, S.N., Browning, J., Davies, M.G., et al. (1999). Cationic lipid-mediated CFTR gene transfer to the lungs and nose of patients with cystic fibrosis: a double-blind placebo-controlled trial. Lancet *353*, 947–954. https://doi.org/10.1016/s0140-6736(98)06532-5.

47. Pei, Y., Bao, Y., Sacchetti, C., Brady, J., Gillard, K., Yu, H., Roberts, S., Rajappan, K., Tanis, S.P., Perez-Garcia, C.G., et al. (2022). Synthesis and bioactivity of readily hydrolysable novel cationic lipids for potential lung delivery application of mRNAs. Chem. Phys. Lipids *243*, 105178. https://doi.org/10.1016/j.chemphyslip.2022.105178.

48. Wang, Y., Zhang, J., Liu, Y., Yue, X., Han, K., Kong, Z., Dong, Y., Yang, Z., Fu, Z., Tang, C., et al. (2024). Realveolarization with inhalable mucus-penetrating lipid nanoparticles for the treatment of pulmonary fibrosis in mice. Sci. Adv. *10*, eado4791. https://doi.org/10.1126/sciadv.ado4791.

49. Lewis, M.M., Soto, M.R., Maier, E.Y., Wulfe, S.D., Bakheet, S., Obregon, H., and Ghosh, D. (2023). Optimization of ionizable lipids for aerosolizable mRNA lipid nanoparticles. Bioeng. Transl. Med. *8*, e10580. https://doi.org/10.1002/btm2.10580.

50. Jiang, A.Y., Witten, J., Raji, I.O., Eweje, F., MacIsaac, C., Meng, S., Oladimeji, F.A., Hu, Y., Manan, R.S., Langer, R., and Anderson, D.G. (2024). Combinatorial development of nebulized mRNA delivery formulations for the lungs. Nat. Nanotechnol. *19*, 364–375. https://doi.org/10.1038/s41565-023-01548-3.

51. Osman, G., Rodriguez, J., Chan, S.Y., Chisholm, J., Duncan, G., Kim, N., Tatler, A.L., Shakesheff, K.M., Hanes, J., Suk, J.S., and Dixon, J.E. (2018). PEGylated enhanced cell penetrating peptide nanoparticles for lung gene therapy. J. Contr. Release *285*, 35–45. https://doi.org/10.1016/j.jconrel.2018.07.001.

52. Randell, S.H., Fulcher, M.L., O'Neal, W., and Olsen, J.C. (2011). Primary Epithelial Cell Models for Cystic Fibrosis Research. In Cystic Fibrosis: Diagnosis and Protocols, Volume II: Methods and Resources to Understand Cystic Fibrosis, M.D. Amaral and K. Kunzelmann, eds. (Humana Press), pp. 285–310. https://doi.org/10.1007/978-1-61779-120-8_18.

53. Bosquillon, C., Madlova, M., Patel, N., Clear, N., and Forbes, B. (2017). A Comparison of Drug Transport in Pulmonary Absorption Models: Isolated Perfused rat Lungs, Respiratory Epithelial Cell Lines and Primary Cell Culture. Pharm. Res. (N. Y.) *34*, 2532–2540. https://doi.org/10.1007/s11095-017-2251-y.

54. Rayner, R.E., Makena, P., Prasad, G.L., and Cormet-Boyaka, E. (2019). Optimization of Normal Human Bronchial Epithelial (NHBE) Cell 3D Cultures for in vitro Lung Model Studies. Sci. Rep. *9*, 500. https://doi.org/10.1038/s41598-018-36735-z.

55. Rayner, R.E., Wellmerling, J., Osman, W., Honesty, S., Alfaro, M., Peeples, M.E., and Cormet-Boyaka, E. (2020). In vitro 3D culture lung model from expanded primary cystic fibrosis human airway cells. J. Cyst. Fibros. *19*, 752–761. https://doi.org/10.1016/j.jcf.2020.05.007.

56. Scudieri, P., Musante, I., Venturini, A., Guidone, D., Genovese, M., Cresta, F., Caci, E., Palleschi, A., Poeta, M., Santamaria, F., et al. (2020). Ionocytes and CFTR Chloride Channel Expression in Normal and Cystic Fibrosis Nasal and Bronchial Epithelial Cells. Cells *9*, 2090. https://doi.org/10.3390/cells9092090.

57. Cidem, A., Bradbury, P., Traini, D., and Ong, H.X. (2020). Modifying and Integrating in vitro and ex vivo Respiratory Models for Inhalation Drug Screening. Front. Bioeng. Biotechnol. *8*, 581995. https://doi.org/10.3389/fbioe.2020.581995.

58. Silva, I.A.L., Laselva, O., and Lopes-Pacheco, M. (2022). Advances in Preclinical In Vitro Models for the Translation of Precision Medicine for Cystic Fibrosis. J. Personalized Med. *12*, 1321. https://doi.org/10.3390/jpm12081321.

59. Stewart, C.E., Torr, E.E., Mohd Jamili, N.H., Bosquillon, C., and Sayers, I. (2012). Evaluation of differentiated human bronchial epithelial cell culture systems for asthma research. J. Allergy *2012*, 943982. https://doi.org/10.1155/2012/943982.

60. Herman, R.E., Makienko, E.G., Prieve, M.G., Fuller, M., Houston, M.E., Jr., and Johnson, P.H. (2007). Phage display screening of epithelial cell monolayers treated with EGTA: identification of peptide FDFWITP that modulates tight junction activity. J. Biomol. Screen *12*, 1092–1101. https://doi.org/10.1177/1087057107310216.

61. Dennis, M.S. (2015). Selection and Screening Strategies, 2 Edition. In Phage Display in Biotechnology and Drug Discovery, S.S. Sidhu and C.R. Geyer, eds. (CRC Press), pp. 97–111.

62. Barry, M.A., Dower, W.J., and Johnston, S.A. (1996). Toward cell-targeting gene therapy vectors: selection of cell-binding peptides from random peptide-presenting phage libraries. Nat. Med. *2*, 299–305. https://doi.org/10.1038/nm0396-299.

63. Kumari, A., Pal, S., G, B.R., Mohny, F.P., Gupta, N., Miglani, C., Pattnaik, B., Pal, A., and Ganguli, M. (2022). Surface-Engineered Mucus Penetrating Nucleic Acid Delivery Systems with Cell Penetrating Peptides for the Lungs. Mol. Pharm. *19*, 1309–1324. https://doi.org/10.1021/acs.molpharmaceut.1c00770.

64. Schuster, B.S., Suk, J.S., Woodworth, G.F., and Hanes, J. (2013). Nanoparticle diffusion in respiratory mucus from humans without lung disease. Biomaterials *34*, 3439–3446. https://doi.org/10.1016/j.biomaterials.2013.01.064.

65. Xu, Q., Ensign, L.M., Boylan, N.J., Schön, A., Gong, X., Yang, J.C., Lamb, N.W., Cai, S., Yu, T., Freire, E., and Hanes, J. (2015). Impact of Surface Polyethylene Glycol (PEG) Density on Biodegradable Nanoparticle Transport in Mucus ex Vivo and Distribution in Vivo. ACS Nano *9*, 9217–9227. https://doi.org/10.1021/acsnano.5b03876.

66. Maisel, K., Reddy, M., Xu, Q., Chattopadhyay, S., Cone, R., Ensign, L.M., and Hanes, J. (2016). Nanoparticles coated with high molecular weight PEG penetrate mucus and provide uniform vaginal and colorectal distribution in vivo. Nanomedicine *11*, 1337–1343. https://doi.org/10.2217/nnm-2016-0047.

67. Li, H., Guissi, N.E.I., Su, Z., Ping, Q., and Sun, M. (2016). Effects of surface hydrophilic properties of PEG-based mucus-penetrating nanostructured lipid carriers on oral drug delivery. RSC Adv. *6*, 84164–84176. https://doi.org/10.1039/c6ra18724b.

68. Schneider, C.S., Xu, Q., Boylan, N.J., Chisholm, J., Tang, B.C., Schuster, B.S., Henning, A., Ensign, L.M., Lee, E., Adstamongkonkul, P., et al. (2017). Nanoparticles that do not adhere to mucus provide uniform and long-lasting drug delivery to airways following inhalation. Sci. Adv. *3*, e1601556. https://doi.org/10.1126/sciadv.1601556.

69. Li, P., Chen, X., Shen, Y., Li, H., Zou, Y., Yuan, G., Hu, P., and Hu, H. (2019). Mucus penetration enhanced lipid polymer nanoparticles improve the eradication rate of Helicobacter pylori biofilm. J. Contr. Release *300*, 52–63. https://doi.org/10.1016/j.jconrel.2019.02.039.

70. Qiu, Y., Man, R.C.H., Liao, Q., Kung, K.L.K., Chow, M.Y.T., and Lam, J.K.W. (2019). Effective mRNA pulmonary delivery by dry powder formulation of PEGylated synthetic KL4 peptide. J. Contr. Release *314*, 102–115. https://doi.org/10.1016/j.jconrel.2019.10.026.

71. Futaki, S., Suzuki, T., Ohashi, W., Yagami, T., Tanaka, S., Ueda, K., and Sugiura, Y. (2001). Arginine-rich peptides. An abundant source of membrane-permeable peptides having potential as carriers for intracellular protein delivery. J. Biol. Chem. *276*, 5836–5840. https://doi.org/10.1074/jbc.M007540200.

72. Milletti, F. (2012). Cell-penetrating peptides: classes, origin, and current landscape. Drug Discov. Today *17*, 850–860. https://doi.org/10.1016/j.drudis.2012.03.002.

73. Li, L.D., Crouzier, T., Sarkar, A., Dunphy, L., Han, J., and Ribbeck, K. (2013). Spatial configuration and composition of charge modulates transport into a mucin hydrogel barrier. Biophys. J. *105*, 1357–1365. https://doi.org/10.1016/j.bpj.2013.07.050.

74. Vedadghavami, A., Wagner, E.K., Mehta, S., He, T., Zhang, C., and Bajpayee, A.G. (2019). Cartilage penetrating cationic peptide carriers for applications in drug delivery to avascular negatively charged tissues. Acta Biomater. *93*, 258–269. https://doi.org/10.1016/j.actbio.2018.12.004.

75. Marczynski, M., Käsdorf, B.T., Altaner, B., Wenzler, A., Gerland, U., and Lieleg, O. (2018). Transient binding promotes molecule penetration into mucin hydrogels by enhancing molecular partitioning. Biomater. Sci. *6*, 3373–3387. https://doi.org/10.1039/c8bm00664d.

76. Cheng, Q., Wei, T., Farbiak, L., Johnson, L.T., Dilliard, S.A., and Siegwart, D.J. (2020). Selective organ targeting (SORT) nanoparticles for tissue-specific mRNA delivery and CRISPR-Cas gene editing. Nat. Nanotechnol. *15*, 313–320. https://doi.org/10.1038/s41565-020-0669-6.

77. Kwon, E.J., Skalak, M., Lo Bu, R., and Bhatia, S.N. (2016). Neuron-Targeted Nanoparticle for siRNA Delivery to Traumatic Brain Injuries. ACS Nano *10*, 7926–7933. https://doi.org/10.1021/acsnano.6b03858.

78. Lo, J.H., Hao, L., Muzumdar, M.D., Raghavan, S., Kwon, E.J., Pulver, E.M., Hsu, F., Aguirre, A.J., Wolpin, B.M., Fuchs, C.S., et al. (2018). iRGD-guided Tumor-penetrating Nanocomplexes for Therapeutic siRNA Delivery to Pancreatic Cancer. Mol. Cancer Therapeut. *17*, 2377–2388. https://doi.org/10.1158/1535-7163.MCT-17-1090.

79. Jain, P.K., Lo, J.H., Rananaware, S., Downing, M., Panda, A., Tai, M., Raghavan, S., Fleming, H.E., and Bhatia, S.N. (2019). Non-viral delivery of CRISPR/Cas9 complex using CRISPR-GPS nanocomplexes. Nanoscale *11*, 21317–21323. https://doi.org/10.1039/c9nr01786k.

80. Munir, M., Kett, V.L., Dunne, N.J., and McCarthy, H.O. (2022). Development of a Spray-Dried Formulation of Peptide-DNA Nanoparticles into a Dry Powder for Pulmonary Delivery Using Factorial Design. Pharm. Res. (N. Y.) *39*, 1215–1232. https://doi.org/10.1007/s11095-022-03256-4.

81. Herrera-Barrera, M., Ryals, R.C., Gautam, M., Jozic, A., Landry, M., Korzun, T., Gupta, M., Acosta, C., Stoddard, J., Reynaga, R., et al. (2023). Peptide-guided lipid nanoparticles deliver mRNA to the neural retina of rodents and nonhuman primates. Sci. Adv. *9*, eadd4623. https://doi.org/10.1126/sciadv.add4623.

82. Anthiya, S., Öztürk, S.C., Yanik, H., Tavukcuoglu, E., Şahin, A., Datta, D., Charisse, K., Álvarez, D.M., Loza, M.I., Calvo, A., et al. (2023). Targeted siRNA lipid nanoparticles for the treatment of KRAS-mutant tumors. J. Contr. Release *357*, 67–83. https://doi.org/10.1016/j.jconrel.2023.03.016.

83. Qin, J., Xue, L., Gong, N., Zhang, H., Shepherd, S.J., Haley, R.M., Swingle, K.L., and Mitchell, M.J. (2022). RGD peptide-based lipids for targeted mRNA delivery and gene editing applications. RSC Adv. *12*, 25397–25404. https://doi.org/10.1039/d2ra02771b.

84. Hisert, K.B., Liles, W.C., and Manicone, A.M. (2019). A Flow Cytometric Method for Isolating Cystic Fibrosis Airway Macrophages from Expectorated Sputum. Am. J. Respir. Cell Mol. Biol. *61*, 42–50. https://doi.org/10.1165/rcmb.2018-0236MA.

85. Hou, F., Xiao, K., Tang, L., and Xie, L. (2021). Diversity of Macrophages in Lung Homeostasis and Diseases. Front. Immunol. *12*, 753940. https://doi.org/10.3389/fimmu.2021.753940.

86. Wright, A.K.A., Rao, S., Range, S., Eder, C., Hofer, T.P.J., Frankenberger, M., Kobzik, L., Brightling, C., Grigg, J., and Ziegler-Heitbrock, L. (2009). Pivotal Advance: Expansion of small sputum macrophages in CF: failure to express MARCO and mannose receptors. J. Leukoc. Biol. *86*, 479–489. https://doi.org/10.1189/jlb.1108699.

87. Murphy, B.S., Bush, H.M., Sundareshan, V., Davis, C., Hagadone, J., Cory, T.J., Hoy, H., Hayes, D., Jr., Anstead, M.I., and Feola, D.J. (2010). Characterization of macrophage activation states in patients with cystic fibrosis. J. Cyst. Fibros. *9*, 314–322. https://doi.org/10.1016/j.jcf.2010.04.006.

88. Ruge, C.A., Kirch, J., Cañadas, O., Schneider, M., Perez-Gil, J., Schaefer, U.F., Casals, C., and Lehr, C.M. (2011). Uptake of nanoparticles by alveolar macrophages is triggered by surfactant protein A. Nanomedicine *7*, 690–693. https://doi.org/10.1016/j.nano.2011.07.009.

89. Ruge, C.A., Schaefer, U.F., Herrmann, J., Kirch, J., Cañadas, O., Echaide, M., Pérez-Gil, J., Casals, C., Müller, R., and Lehr, C.M. (2012). The interplay of lung surfactant proteins and lipids assimilates the macrophage clearance of nanoparticles. PLoS One *7*, e40775. https://doi.org/10.1371/journal.pone.0040775.

90. Geiser, M., Quaile, O., Wenk, A., Wigge, C., Eigeldinger-Berthou, S., Hirn, S., Schäffler, M., Schleh, C., Möller, W., Mall, M.A., and Kreyling, W.G. (2013). Cellular uptake and localization of inhaled gold nanoparticles in lungs of mice with chronic obstructive pulmonary disease. Part. Fibre Toxicol. *10*, 19. https://doi.org/10.1186/1743-8977-10-19.

91. Yin, B., Chan, C.K.W., Liu, S., Hong, H., Wong, S.H.D., Lee, L.K.C., Ho, L.W.C., Zhang, L., Leung, K.C.F., Choi, P.C.L., et al. (2019). Intrapulmonary Cellular-Level Distribution of Inhaled Nanoparticles with Defined Functional Groups and Its Correlations with Protein Corona and Inflammatory Response. ACS Nano *13*, 14048–14069. https://doi.org/10.1021/acsnano.9b06424.

92. Lokugamage, M.P., Vanover, D., Beyersdorf, J., Hatit, M.Z.C., Rotolo, L., Echeverri, E.S., Peck, H.E., Ni, H., Yoon, J.K., Kim, Y., et al. (2021). Optimization of lipid nanoparticles for the delivery of nebulized therapeutic mRNA to the lungs. Nat. Biomed. Eng. *5*, 1059–1068. https://doi.org/10.1038/s41551-021-00786-x.

93. Shimosakai, R., Khalil, I.A., Kimura, S., and Harashima, H. (2022). mRNA-Loaded Lipid Nanoparticles Targeting Immune Cells in the Spleen for Use as Cancer Vaccines. Pharmaceuticals *15*, 1017. https://doi.org/10.3390/ph15081017.

94. Leppek, K., Byeon, G.W., Kladwang, W., Wayment-Steele, H.K., Kerr, C.H., Xu, A.F., Kim, D.S., Topkar, V.V., Choe, C., Rothschild, D., et al. (2022). Combinatorial optimization of mRNA structure, stability, and translation for RNA-based therapeutics. Nat. Commun. *13*, 1536. https://doi.org/10.1038/s41467-022-28776-w.

95. Kimura, S., and Harashima, H. (2023). On the mechanism of tissue-selective gene delivery by lipid nanoparticles. J. Contr. Release *362*, 797–811. https://doi.org/10.1016/j.jconrel.2023.03.052.

96. Huayamares, S.G., Lokugamage, M.P., Rab, R., Da Silva Sanchez, A.J., Kim, H., Radmand, A., Loughrey, D., Lian, L., Hou, Y., Achyut, B.R., et al. (2023). High-throughput screens identify a lipid nanoparticle that preferentially delivers mRNA to human tumors in vivo. J. Contr. Release *357*, 394–403. https://doi.org/10.1016/j.jconrel.2023.04.005.

97. Kim, M., Jeong, M., Lee, G., Lee, Y., Park, J., Jung, H., Im, S., Yang, J.S., Kim, K., and Lee, H. (2023). Novel piperazine-based ionizable lipid nanoparticles allow the repeated dose of mRNA to fibrotic lungs with improved potency and safety. Bioeng. Transl. Med. *8*, e10556. https://doi.org/10.1002/btm2.10556.

98. Sousa, A.A., Hemez, C., Lei, L., Traore, S., Kulhankova, K., Newby, G.A., Doman, J.L., Oye, K., Pandey, S., Karp, P.H., et al. (2024). Systematic optimization of prime editing for the efficient functional correction of CFTR F508del in human airway epithelial cells. Nat. Biomed. Eng. https://doi.org/10.1038/s41551-024-01233-3.

99. Ramalho, A.S., Beck, S., Meyer, M., Penque, D., Cutting, G.R., and Amaral, M.D. (2002). Five percent of normal cystic fibrosis transmembrane conductance regulator mRNA ameliorates the severity of pulmonary disease in cystic fibrosis. Am. J. Respir. Cell Mol. Biol. *27*, 619–627. https://doi.org/10.1165/rcmb.2001-0004OC.

100. Cooney, A.L., Abou Alaiwa, M.H., Shah, V.S., Bouzek, D.C., Stroik, M.R., Powers, L.S., Gansemer, N.D., Meyerholz, D.K., Welsh, M.J., Stoltz, D.A., et al. (2016). Lentiviral-mediated phenotypic correction of cystic fibrosis pigs. JCI Insight *1*, e88730. https://doi.org/10.1172/jci.insight.88730.

101. Okuda, K., Dang, H., Kobayashi, Y., Carraro, G., Nakano, S., Chen, G., Kato, T., Asakura, T., Gilmore, R.C., Morton, L.C., et al. (2021). Secretory Cells Dominate

Airway CFTR Expression and Function in Human Airway Superficial Epithelia. Am. J. Respir. Crit. Care Med. *203*, 1275–1289. https://doi.org/10.1164/rccm.202008-3198OC.

102. Voynow, J.A., Fischer, B.M., Roberts, B.C., and Proia, A.D. (2005). Basal-like cells constitute the proliferating cell population in cystic fibrosis airways. Am. J. Respir. Crit. Care Med. *172*, 1013–1018. https://doi.org/10.1164/rccm.200410-1398OC.

103. Montoro, D.T., Haber, A.L., Biton, M., Vinarsky, V., Lin, B., Birket, S.E., Yuan, F., Chen, S., Leung, H.M., Villoria, J., et al. (2018). A revised airway epithelial hierarchy includes CFTR-expressing ionocytes. Nature *560*, 319–324. https://doi.org/10.1038/s41586-018-0393-7.

104. Smith, G.P., and Scott, J.K. (1993). Libraries of peptides and proteins displayed on filamentous phage. Methods Enzymol. *217*, 228–257. https://doi.org/10.1016/0076-6879(93)17065-d.

105. Donaldson, S.H., Bennett, W.D., Zeman, K.L., Knowles, M.R., Tarran, R., and Boucher, R.C. (2006). Mucus clearance and lung function in cystic fibrosis with hypertonic saline. N. Engl. J. Med. *354*, 241–250. https://doi.org/10.1056/NEJMoa043891.

106. Lindstrom, M., Camner, P., Falk, R., Hjelte, L., Philipson, K., and Svartengren, M. (2005). Long-term clearance from small airways in patients with cystic fibrosis. Eur. Respir. J. *25*, 317–323. https://doi.org/10.1183/09031936.05.00120103.

107. Liu, G.W., Livesay, B.R., Kacherovsky, N.A., Cieslewicz, M., Lutz, E., Waalkes, A., Jensen, M.C., Salipante, S.J., and Pun, S.H. (2015). Efficient Identification of Murine M2 Macrophage Peptide Targeting Ligands by Phage Display and Next-Generation Sequencing. Bioconjugate Chem. *26*, 1811–1817. https://doi.org/10.1021/acs.bioconjchem.5b00344.

108. Kauffman, K.J., Dorkin, J.R., Yang, J.H., Heartlein, M.W., DeRosa, F., Mir, F.F., Fenton, O.S., and Anderson, D.G. (2015). Optimization of Lipid Nanoparticle Formulations for mRNA Delivery in Vivo with Fractional Factorial and Definitive Screening Designs. Nano Lett. *15*, 7300–7306. https://doi.org/10.1021/acs.nanolett.5b02497.

109. Zeng, C., Hou, X., Yan, J., Zhang, C., Li, W., Zhao, W., Du, S., and Dong, Y. (2020). Leveraging mRNA Sequences and Nanoparticles to Deliver SARS-CoV-2 Antigens In Vivo. Adv. Mater. *32*, e2004452. https://doi.org/10.1002/adma.202004452.

110. Wei, T., Sun, Y., Cheng, Q., Chatterjee, S., Traylor, Z., Johnson, L.T., Coquelin, M.L., Wang, J., Torres, M.J., Lian, X., et al. (2023). Lung SORT LNPs enable precise homology-directed repair mediated CRISPR/Cas genome correction in cystic fibrosis models. Nat. Commun. *14*, 7322. https://doi.org/10.1038/s41467-023-42948-2.